Supplementary Information

Molecular Probes for Tracking Lipid Droplet Membrane Dynamics

Lingxiu Kong[1#], Qingjie Bai[1,2#], Cuicui Li[3,4,5,6#], Qiqin Wang[1,7#], Yanfeng Wang[1], Xintian Shao[1,2,8], Yongchun Wei[1], Jiarao Sun[1], Zhenjie Yu[1], Junling Yin[2], Bin Shi[2,8], Hongbao Fang[9], Xiaoyuan Chen[3,4,5,6,10*], Qixin Chen[1,2,3,5,6,10*]

[1] School of Pharmaceutical Sciences, Shandong First Medical University & Shandong Academy of Medical Sciences, Jinan, Shandong 250117, PR China

[2] Medical Science and Technology Innovation Center, Shandong First Medical University & Shandong Academy of Medical Sciences, Jinan, Shandong 250117, PR China

[3] Departments of Diagnostic Radiology, Surgery, Chemical and Biomolecular Engineering, and Biomedical Engineering, Yong Loo Lin School of Medicine and College of Design and Engineering, National University of Singapore, Singapore 119074, Singapore

[4] Clinical Imaging Research Centre, Centre for Translational Medicine, Yong Loo Lin School of Medicine, National University of Singapore, Singapore 117599, Singapore

[5] Nanomedicine Translational Research Program, Yong Loo Lin School of Medicine, National University of Singapore, Singapore 117597, Singapore

[6] Theranostics Center of Excellence (TCE), Yong Loo Lin School of Medicine, National University of Singapore, 11 Biopolis Way, Helios, Singapore 138667, Singapore

[7] College of Pharmacy, Jinan University, Guangzhou 510632, PR China

[8] Neck-Shoulder and Lumbocrural Pain Hospital, Shandong First Medical University & Shandong Academy of Medical Sciences, Jinan, Shandong 250117, PR China

[9] College of Chemistry and Materials Science, Nanjing Normal University, Nanjing 210023, PR China

[10] Institute of Molecular and Cell Biology, Agency for Science, Technology, and Research (A*STAR), 61 Biopolis Drive, Proteos, Singapore 138673, Singapore

# These authors contributed equally to this work

*Corresponding author. E-mail: chen.shawn@nus.edu.sg (X. Chen); chenqixin@sdfmu.edu.cn (Q. Chen).

Supplementary Figure 29. Fluorescent labeling of LD Membranes by mobile distribution proteins and **LDM**.

Supplementary Figure 30. Membrane of LDs labeled by **LDM** under different resolutions of microscopes.

Supplementary Figure 31. Confocal imaging of **LDM**^{488} (10.0 μM) distribution within cells.

Supplementary Figure 32. SIM co-localization imaging experiment.

Supplementary Figure 33. The size of the LD presented is significantly smaller than the **LDM**^{561}-labeled ring-like structure.

Supplementary Figure 34. Comparison of fluorescence regions between **LDM**^{561} channel membrane imaging and Lipi-B^{405} channel content dye SIM imaging.

Supplementary Figure 35. The differences between membrane protein labeling strategies and content labeling strategies.

Supplementary Figure 36. **LDM**^{561}-labeled red fluorescent molecules show an uneven distribution at the contact site with multiple ring-like structures.

Supplementary Figure 37. The dynamics of Cidec-GFP and **LDM** labeled LD membrane proteins during non-contact and contact periods.

Supplementary Figure 38. SIM images of representative regions of LDs in HepG2 cells labeled with Plin2-mCherry, Plin5-GFP, **LDM**, and Cidec-GFP.

Supplementary Figure 39. SIM imaging of **LDM**^{561} channels of multiple LDs in contact with each other in HepG2 cells.

Supplementary Figure 40. A matching trend between the positioning of Cidec-GFP and the **LDM-OH**-labeled membrane protein in the LD membrane contact area.

Supplementary Figure 41. SIM co localization imaging of HepG2 cells with sodium oleate (100.0 μM).

Supplementary Figure 42. Quantitative analysis of adhesion value changes of WT and sodium oleate in HepG2 cells.

Supplementary Figure 43. Quantitative analysis of changes in adhesion values of WT and FIP200KO in HepG2 cells.

Supplementary Figure 44. LD distribution in WT HeLa cells and ATG13KO HeLa cells.

Supplementary Figure 45. Comparison of TG content in HepG2 cells under serum-fed and serum-free conditions.

Supplementary Figure 46. Representative confocal images of co-localization of C12^{488} and lipi-B^{405} on LD in HepG2 cells.

Supplementary Figure 47. Utilizing **LDM** to assess drug effects on LD and LD interaction

Supplementary Figure 48. Using **LDM** to evaluate the effects and targets of fluorescent drugs on LD

metabolism.

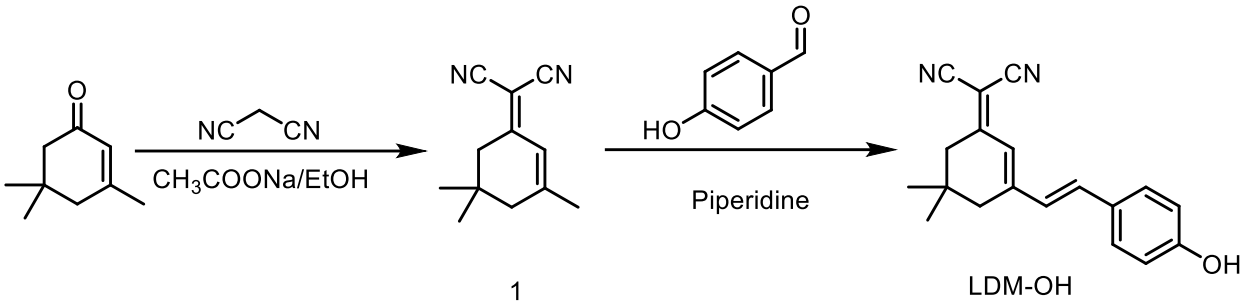

Supplementary Figure 1. Synthesis of **LDM-OH**.

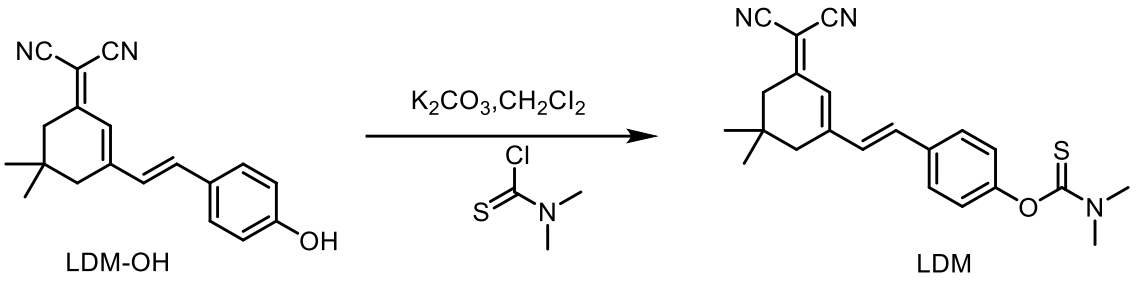

Supplementary Figure 2. Synthesis of **LDM**.

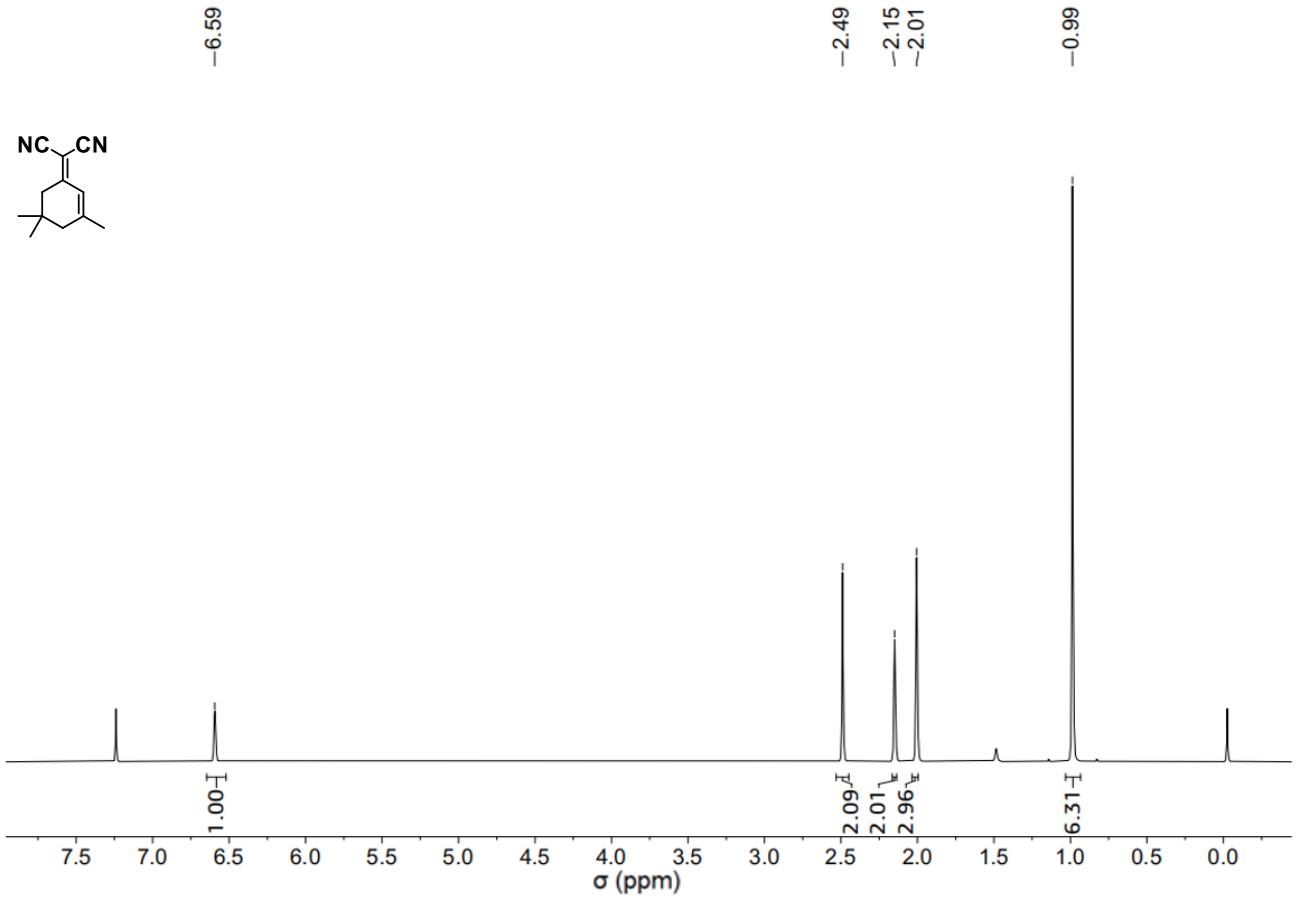

Supplementary Figure 3. ^{1}H NMR spectrum of compound **1** in $CDCl_3$ (400 MHz).

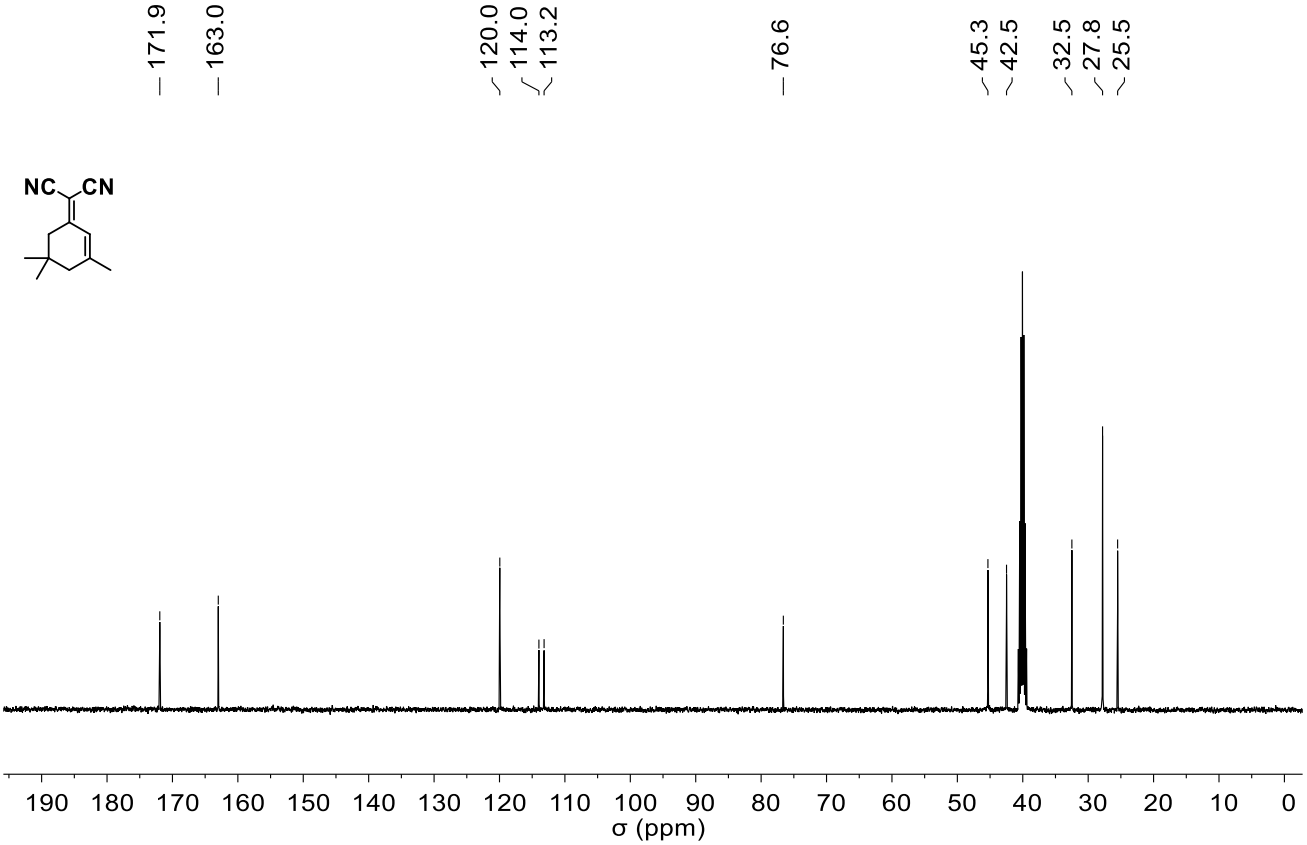

Supplementary Figure 4. ^{13}C-NMR spectra of compound **1** in DMSO- d_6 (101 MHz).

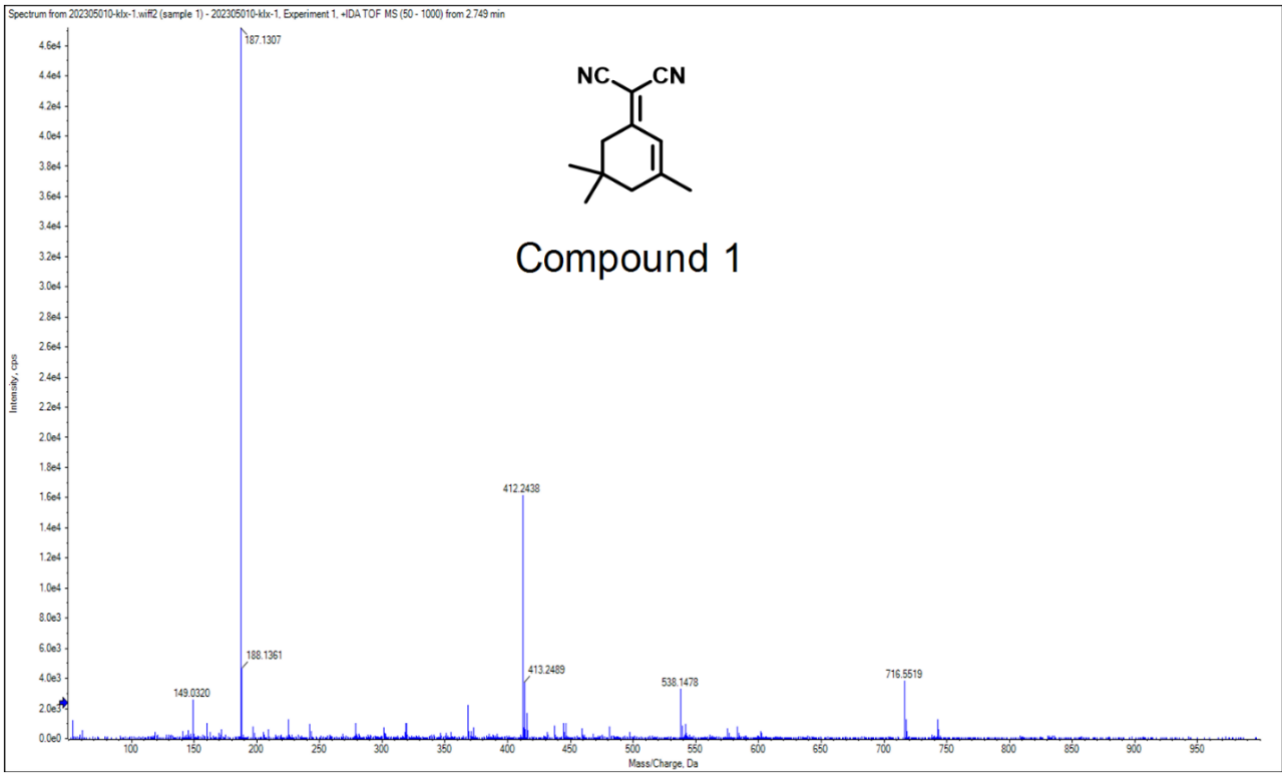

Supplementary Figure 5. LC-HRMS spectrum of compound **1**.

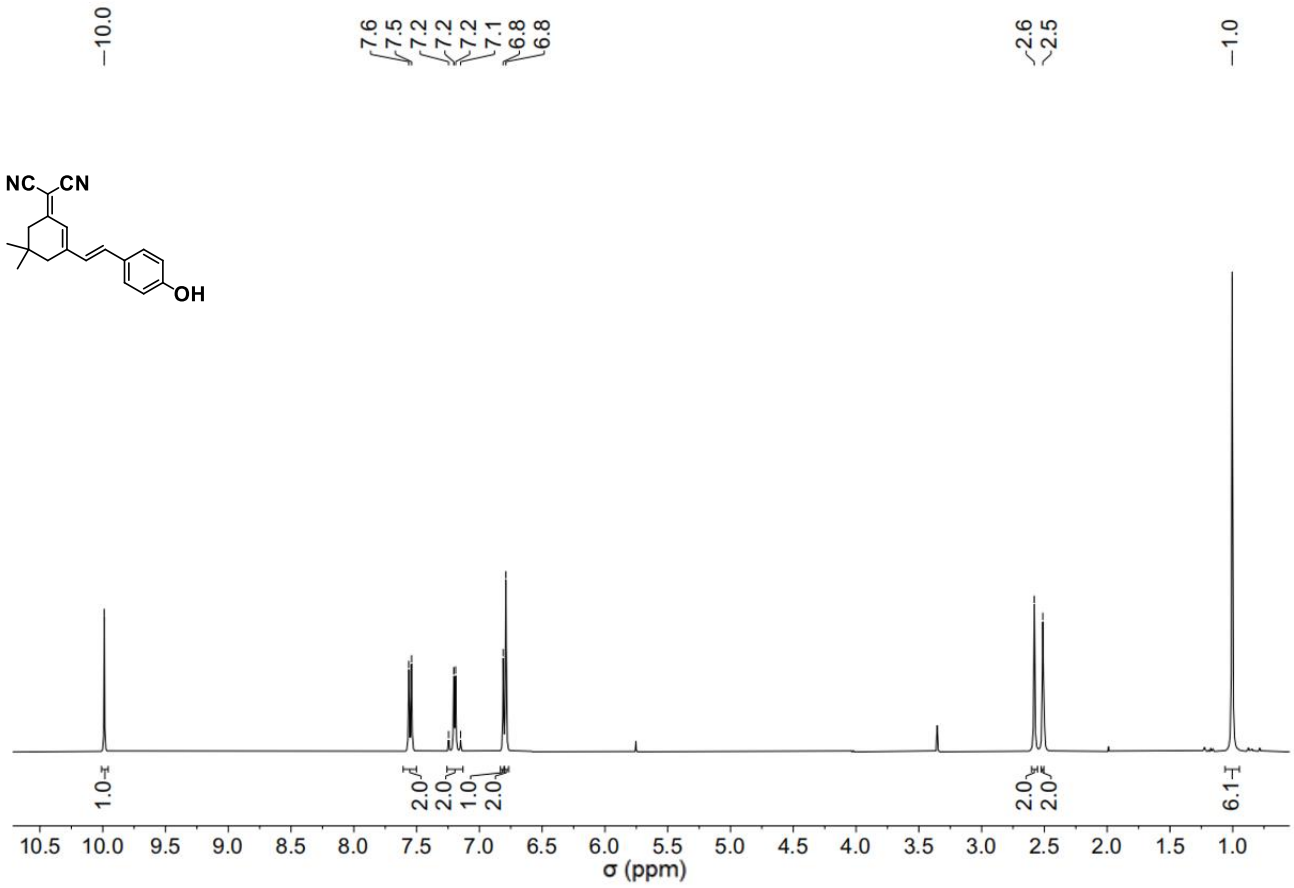

Supplementary Figure 6. ^{1}H NMR spectra of compound **LDM-OH** in DMSO- d_6 (400 MHz).

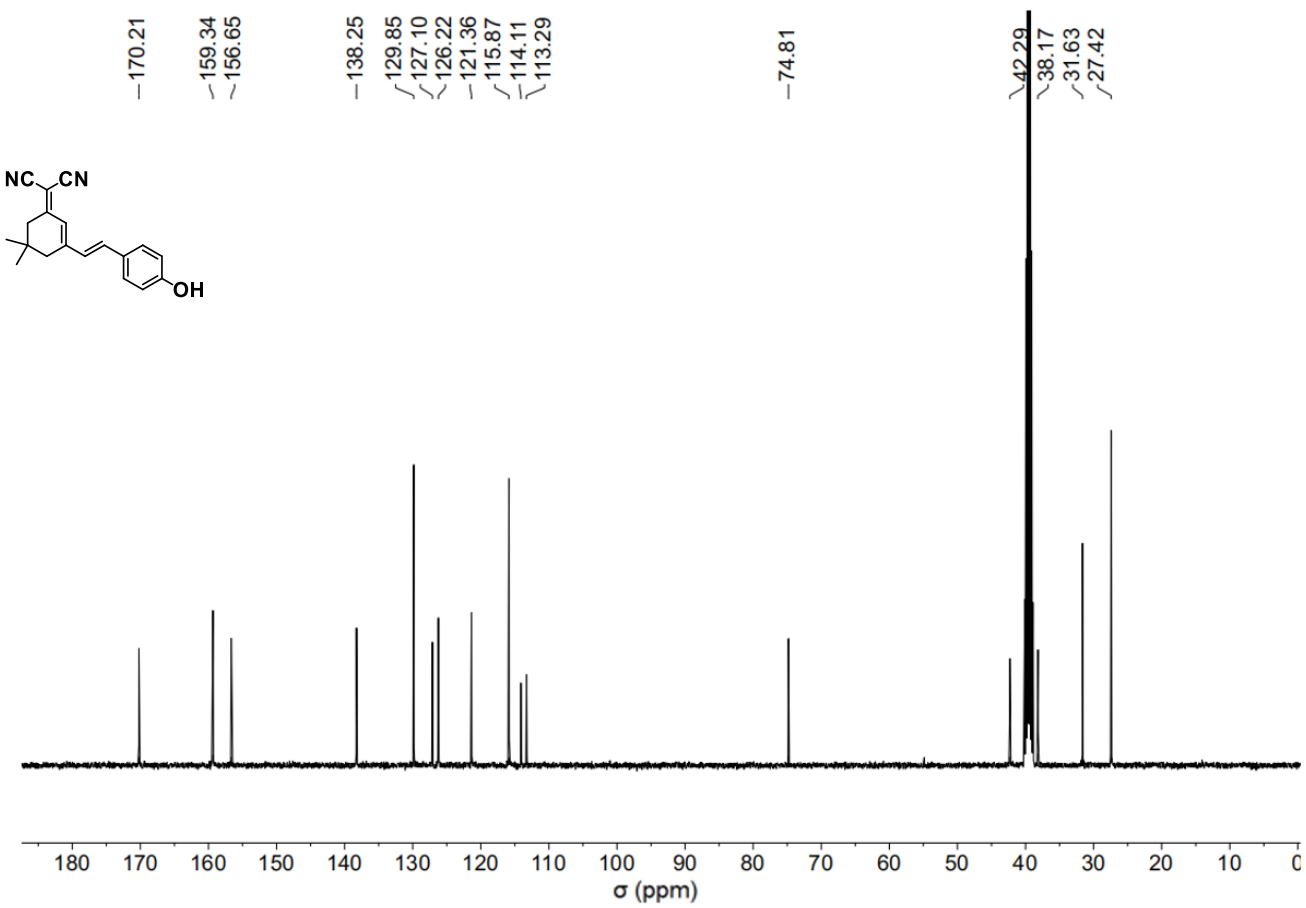

Supplementary Figure 7. ^{13}C-NMR spectra of compound **LDM-OH** in DMSO- d_6 (100 MHz).

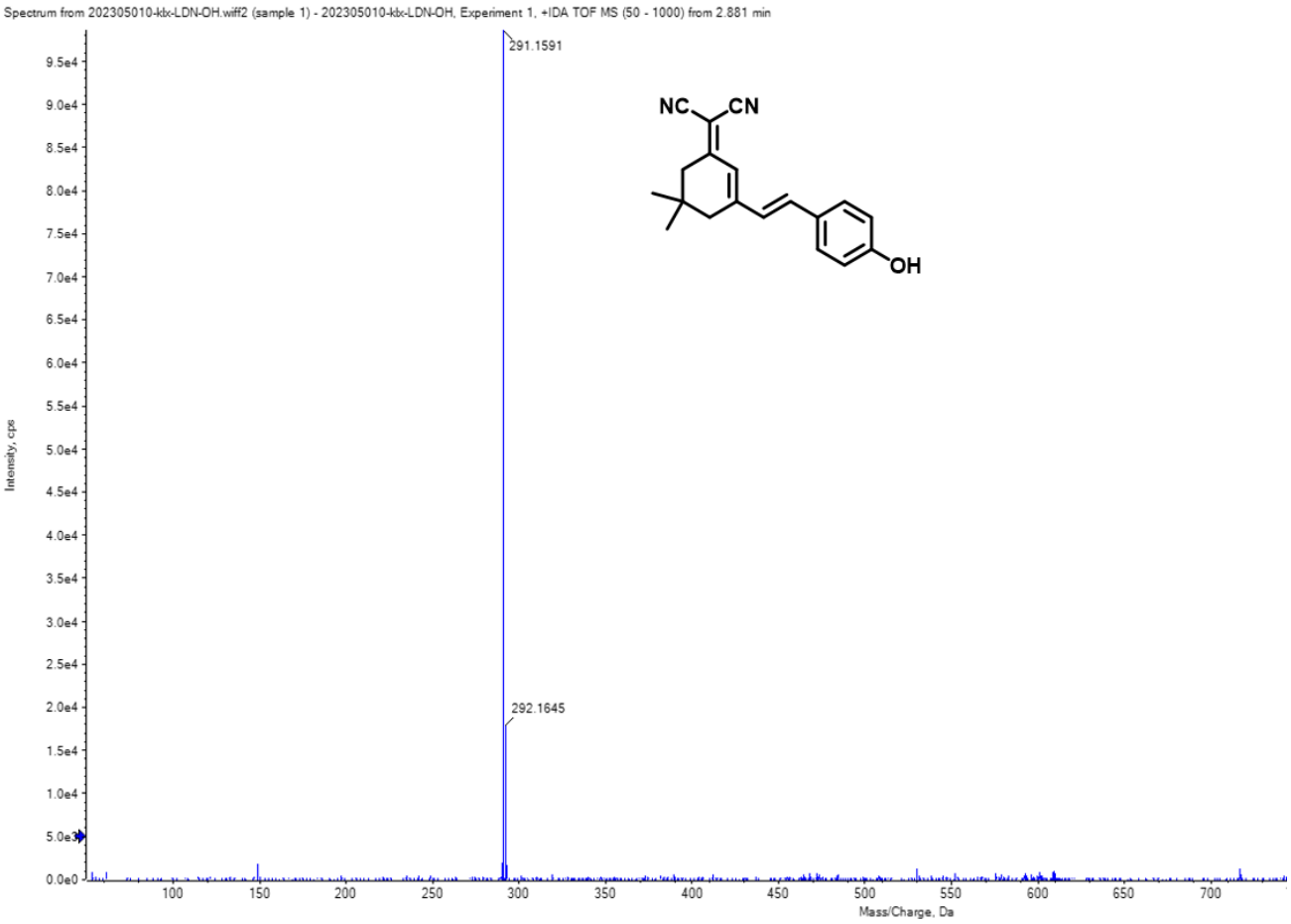

Supplementary Figure 8. LC-HRMS spectra of compound **LDM-OH**.

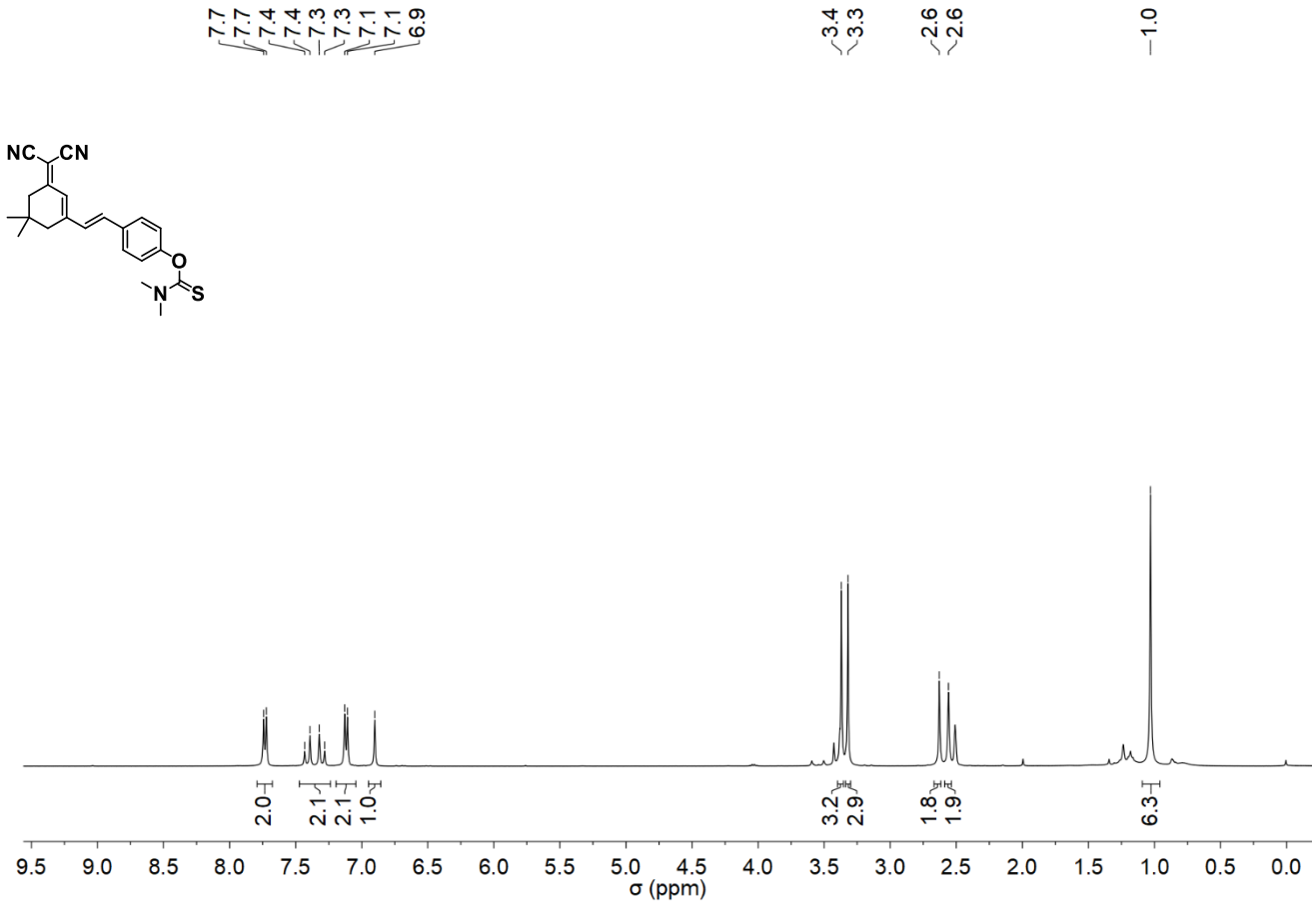

Supplementary Figure 9. ^{1}H NMR spectra of compound **LDM** in DMSO- d_6 (400 MHz).

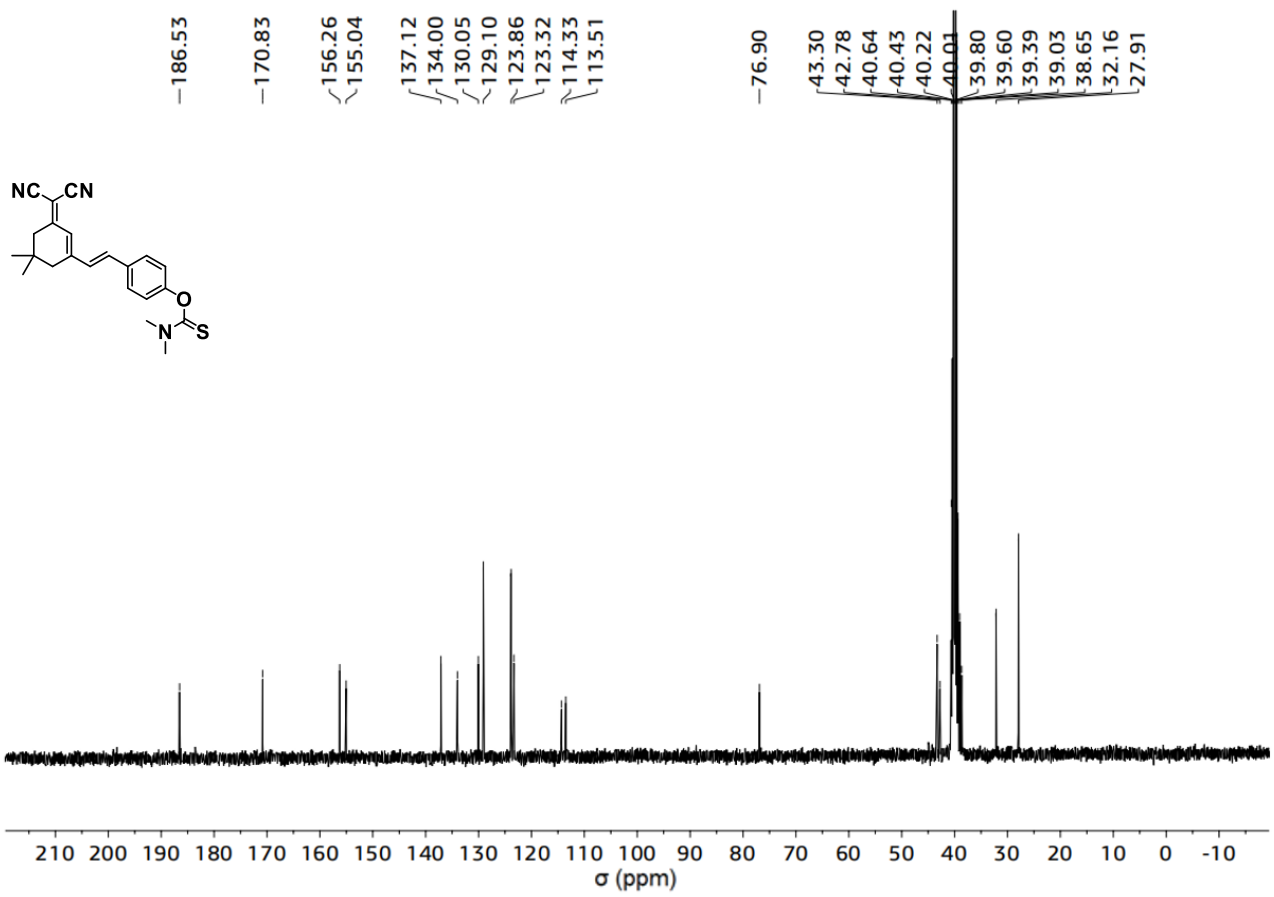

Supplementary Figure 10. ^{13}C-NMR spectra of compound **LDM** in DMSO- d_6 (100 MHz).

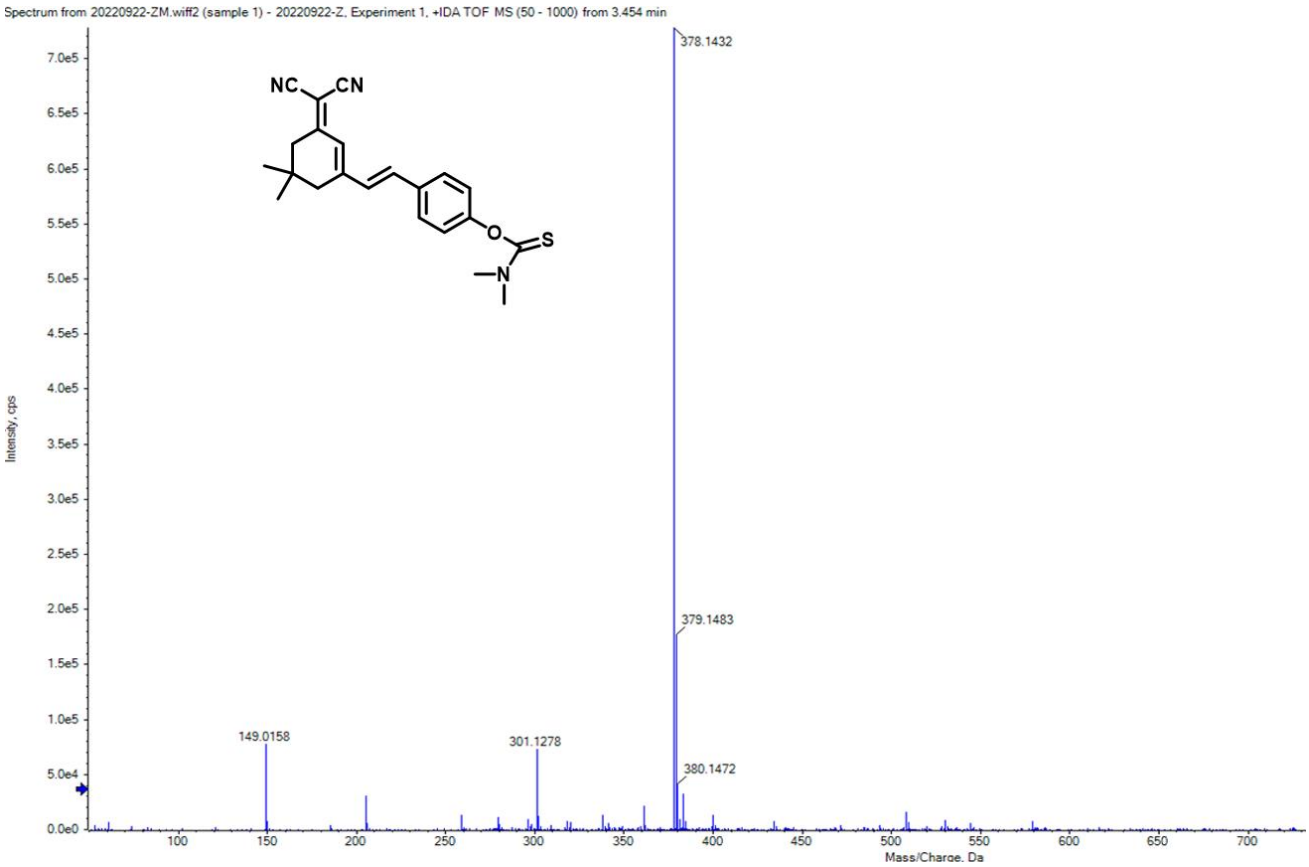

Supplementary Figure 11. LC-HRMS spectra of compound **LDM**.

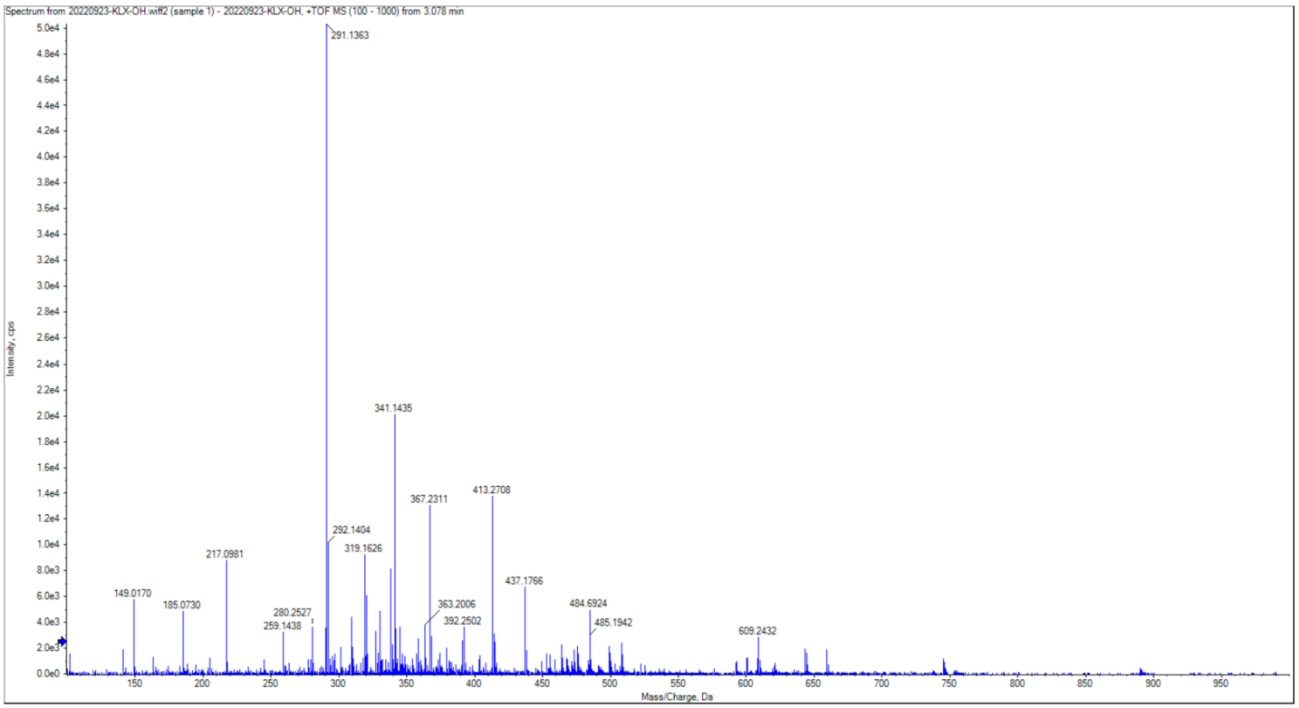

Supplementary Figure 12. The HR-MS diagram of **LDM** (10.0 μM) and ClO^- (100.0 μM) reaction in DMSO-PBS buffer.

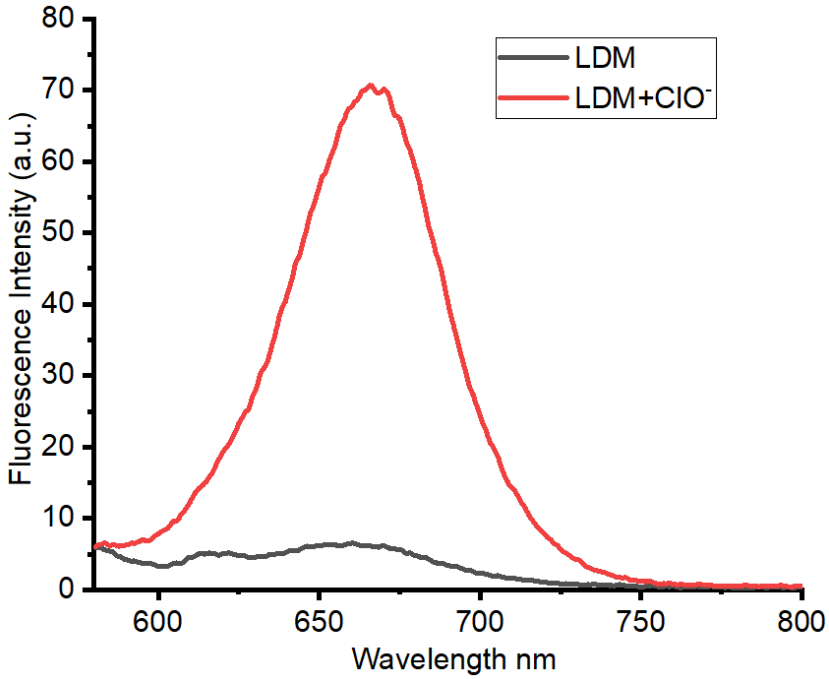

Supplementary Figure 13. Fluorescence spectra of **LDM** itself and with the addition of ClO^- /HClO. **LDM** (10.0 μM) Compared to NaClO (0.0, 100.0 μM) Fluorescence spectra in DMSO-PBS (1:99, v/v, pH = 7.4) solution, λ_{ex} = 561nm, slit: 5nm/5nm/700V. Three independent replicates were performed, and the results were similar. Source data are provided as a source data file.

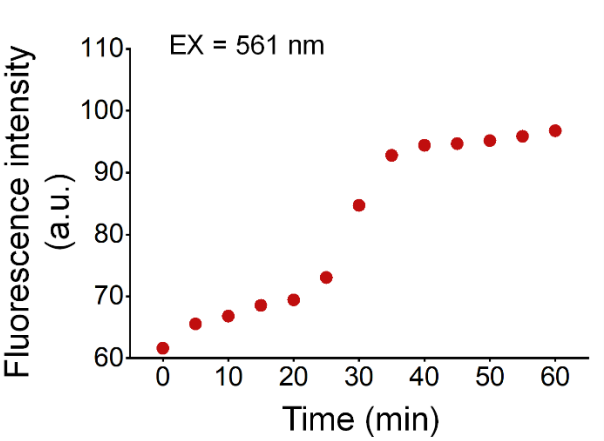

Supplementary Figure 14. The response time between **LDM** and ClO^-. **LDM** (10.0 μM) in different NaClO (100.0 μM) solution (DMSO-PBS, 1:99, v/v, pH = 7.4), λ_{ex} = 561nm, slit: 5 nm/5 nm/700 V, . Three independent replicates were performed, and the results were similar. Source data are provided as a source data file.

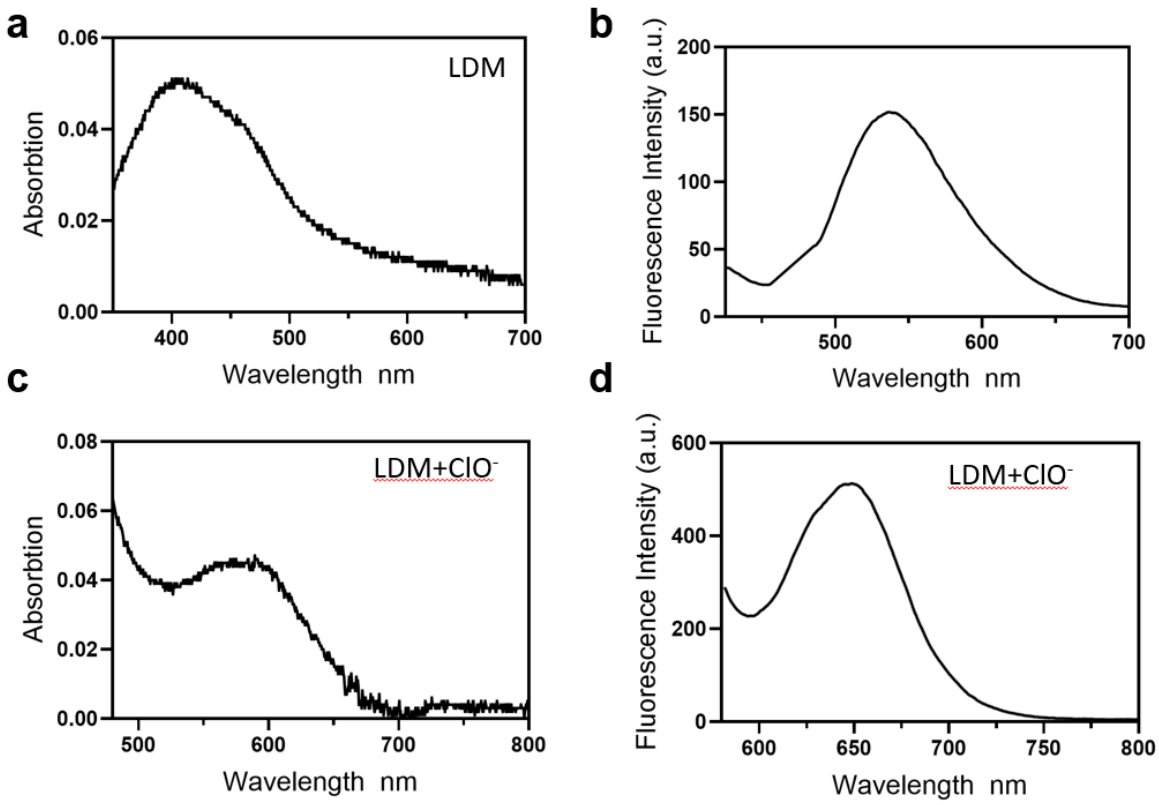

Supplementary Figure 15. Absorption and fluorescence spectra during fluorescence quantum yield measurements. (a) UV absorption spectrum of **LDM** (DMSO-PBS, 1:99, v/v). (b) Fluorescence spectrum of **LDM** in deionized water, λ_{ex} = 405 nm. (c) UV absorption spectrum of **LDM** + ClO^-. (d) Fluorescence spectrum of **LDM** + ClO^-, λ_{ex} = 561 nm. Three independent replicates were performed, and the results were similar. Source data are provided as a source data file.

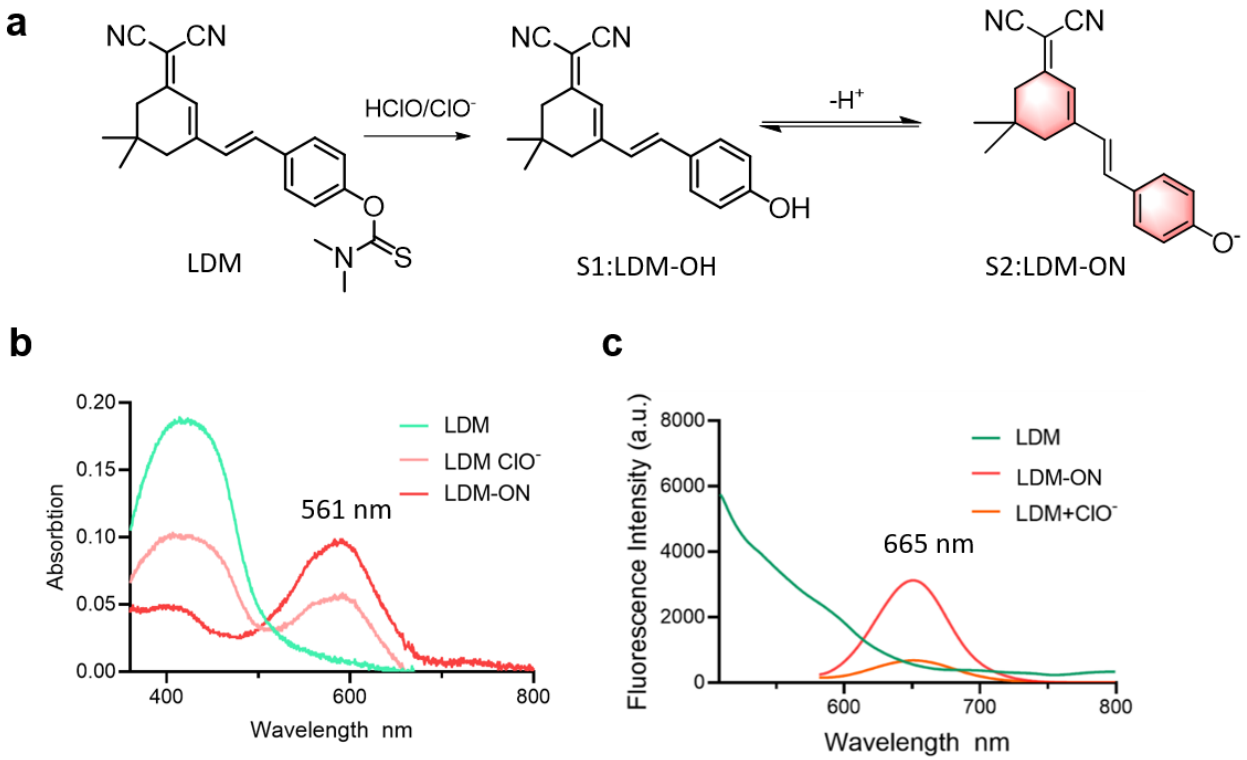

Supplementary Figure 16. (a) The structure of probe **LDM** and its fluorescence response mechanism towards NaClO. (b) The UV spectra changes of **LDM**, **LDM** with additional NaClO and **LDM-ON** (c) The fluorescence spectra changes of **LDM** (10 μM) with additional NaClO (λ_{ex}: 488/561 nm). Three independent replicates were performed, and the results were similar. Source data are provided as a source data file.

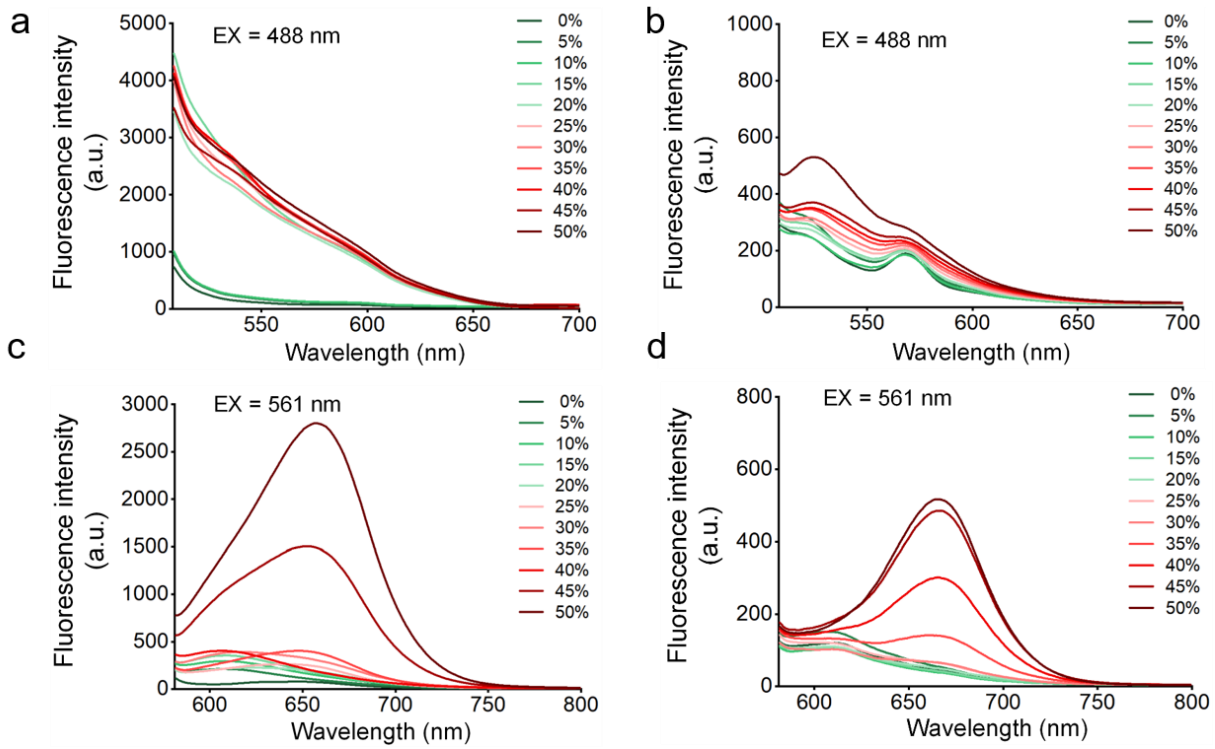

Supplementary Figure 17. The effects of viscosity and polarity on **LDM** and **LDM-OH**. (a) The effect of viscosity (glycerol content) on **LDM**; (b) The effect of polarity (dioxane content) on **LDM**; (c) The effect of viscosity (glycerol content) on **LDM-OH**; (d) The effect of polarity (dioxane content) on **LDM-OH**. **LDM**: λex = 488 nm, slit: 10 nm/10 nm/700 V. **LDM-OH**: λ_{ex} = 561nm, slit: 10 nm/10 nm/700 V. Three independent replicates were performed, and the results were similar. Source data are provided as a source data file.

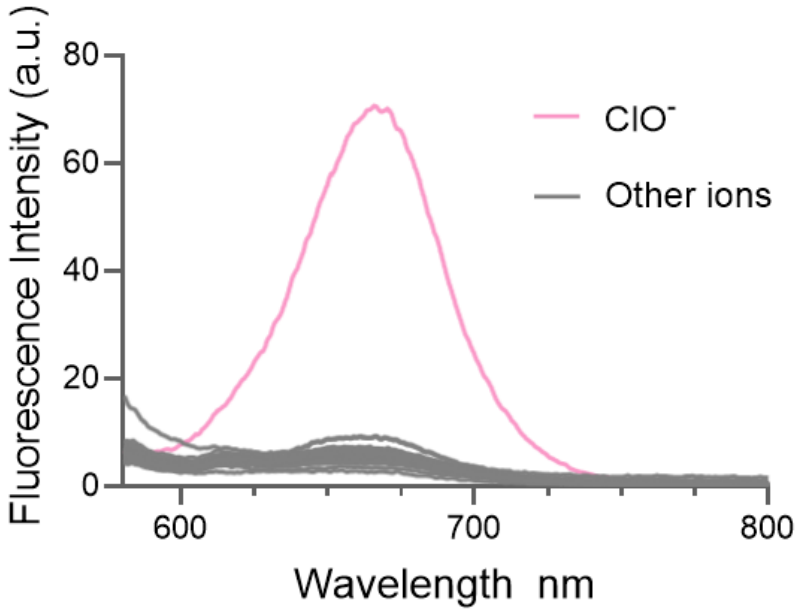

Supplementary Figure 18. Fluorescence spectra of **LDM** with the addition of ions. The fluorescence intensity of mixed solutions of **LDM** and various related substances (100.0 μM). (1.Blank; 2.NO_2^-; 3.t-Buoo$^-$; 4.PO_4^{3-}; 5.•OH; 6.HPO_4^{2-}; 7.CH_3COO^-; 8.F^-; 9.Cl^-; 10.Ag^+; 11.Al^{3+}; 12.Ca^{2+}; 13.Cr^{3+}; 14.Co^{2+}; 15.Fe^{2+}; 16.Fe^{3+}; 17.Mn^{2+}; 18.Ni^{2+}; 19.Pb^{2+}; 20.Zn^{2+}; 21.Cu^{2+}; 22.Hg^{2+}; 23.Cd^{2+}; 24.H_2O_2; 25.NO; 26.SO_4^{2-}; 27.ONOO$^-$; 28.$^1O_2$; 29.ClO^-). Three independent replicates were performed, and the results were similar. Source data are provided as a source data file.

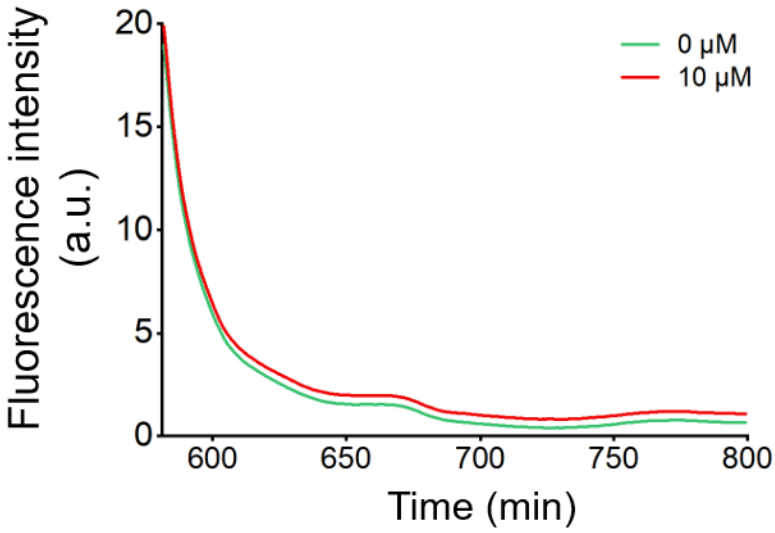

Supplementary Figure19. The response of **LDM** to $\cdot O_2^-$. **LDM** (10.0 μM) in different NaClO (100.0 μM) solution (DMSO-PBS,1:99, v/v, pH = 7.4). λ_{ex} = 561nm, slit: 5 nm/5 nm/700 V. Three independent replicates were performed, and the results were similar. Source data are provided as a source data file.

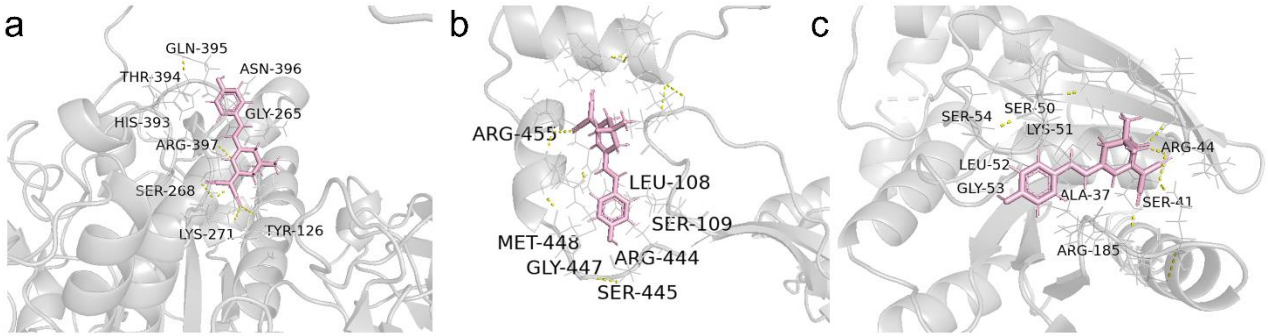

Supplementary Figure 20. Macromolecular docking results of various lipoprotein and **LDM-OH**. The phenolic hydroxyl groups of **LDM-OH** serve as the linking groups for LD membrane proteins. **LDM-OH** binds to proteins (E9Q3E1, Q96KR4, Q9UG22) through hydrogen bonding, hydrophobic interactions, and electrostatic forces. Three independent replicates were performed, and the results

were similar.

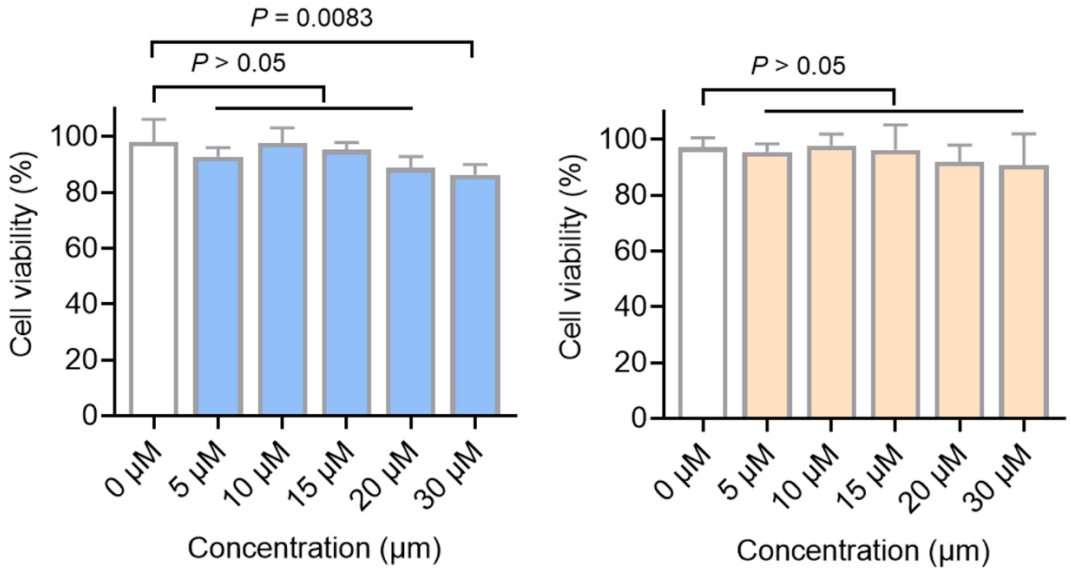

Supplementary Figure 21. The cell survival rate (%) obtained of **LDM** through CCK-8 measurement. HeLa (the left side) and HepG2 (the right side) cells were incubated with different concentrations of **LDM**（0.0 μM, 5.0 μM, 10.0 μM, 20.0 μM, 30.0 μM）for 24 h ($n = 6$ well). Three independent biological replicates were performed, and the results were similar. Statistical analysis was performed using two-tailed unpaired Student's t-test, and the data were presented as mean ± SD. $P < 0.05$ was considered statistically significant. Source data are provided as a source data file.

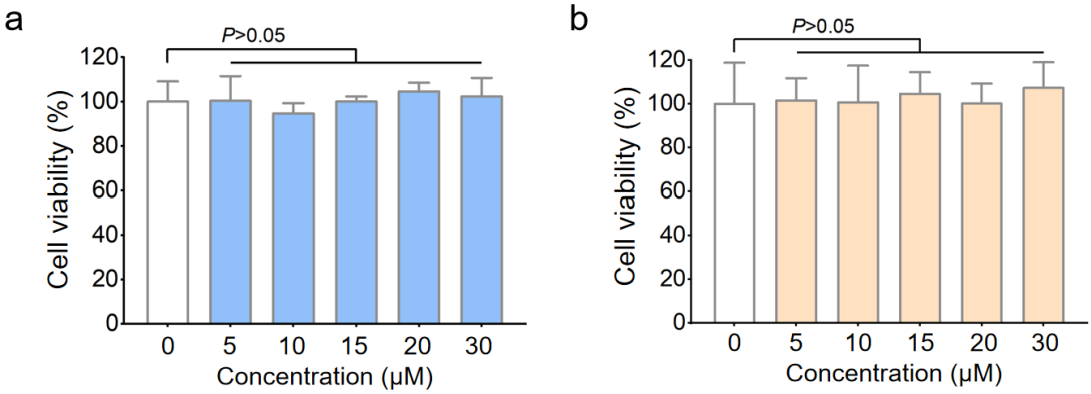

Supplementary Figure 22. The cell survival rate (%) of **LDM-OH** obtained through CCK-8 measurement. HeLa (the left side) and HepG2 (the right side) cells were incubated with different concentrations of **LDM-OH**（0.0 μM, 5.0 μM, 10.0 μM, 20.0 μM, 30.0 μM）for 24 h ($n = 6$ well). Three independent biological replicates were performed, and the results were similar. Statistical analysis was performed using two-tailed unpaired Student's t-test, and the data were presented as mean

± SD. $P < 0.05$ was considered statistically significant. Source data are provided as a source data file.

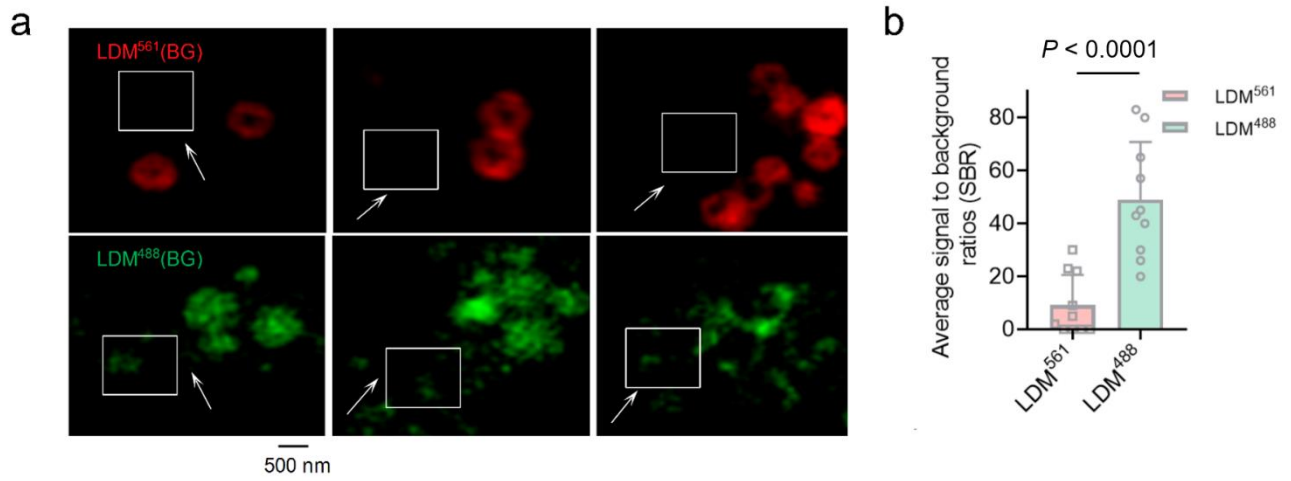

Supplementary Figure 23. Signal and background (BG) regions of **LDM**$^{561/488}$. (a) Merged SIM images of HepG2 cells stained with **LDM**$^{488/561}$ (10.0 μM), with signal and background (BG) regions for each channel indicated. (b) SBRs of **LDM**$^{488/561}$ (n = 10 areas from 5 cells). **LDM**^{488} channel: λ_{ex} = 488 nm; **LDM**^{561} channel: λ_{ex} = 561 nm, scale bars 500 nm. Three independent imaging or biological replicates were performed, and the results were similar. Statistical analysis was performed using two-tailed unpaired Student's t-test, and the data were presented as mean ± SD. $P < 0.05$ was considered statistically significant. Source data are provided as a source data file.

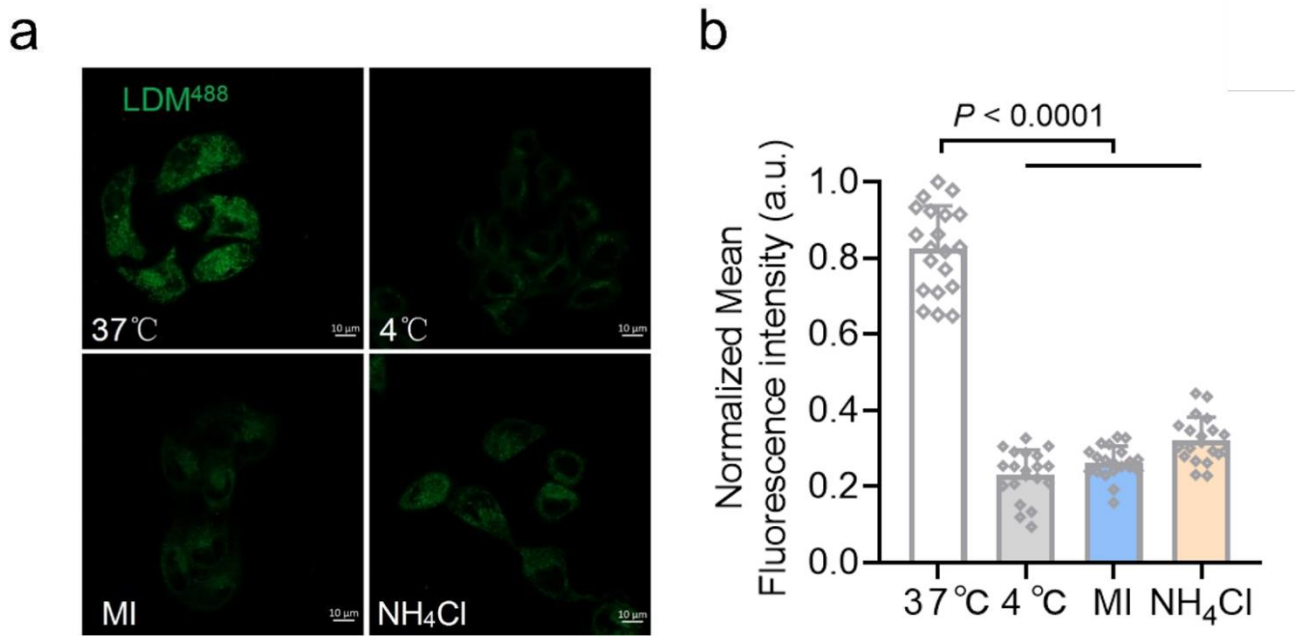

Supplementary Figure 24. Confocal imaging of **LDM** uptake by HepG2 cells. (a) Incubate cells with **LDM** at 37°C for 40 min; Incubate cells with **LDM** at 4°C for 40 min; Incubate cells with metabolic inhibitors (MI) at 37°C with 2-deoxy-D-glucose of 50.0 mM and oligomycin of 5.0 μM was pre

incubated for 1 hour, then incubated with **LDM** at 37°C for 40 min; Cells were pre incubated with 50 mM NH_4Cl at 37°C for 2 h and then incubated with **LDM** at 37°C for 40 min (**LDM**^{488} channel: λ_{ex} = 488 nm; scale bars 10 μm). (b) Quantitative analysis of (a) (n = 20 cells). Three independent imaging replicates were performed, and the results were similar. Statistical analysis was performed using two-tailed unpaired Student's t-test, and the data were presented as mean ± SD. $P < 0.05$ was considered statistically significant. Source data are provided as a source data file.

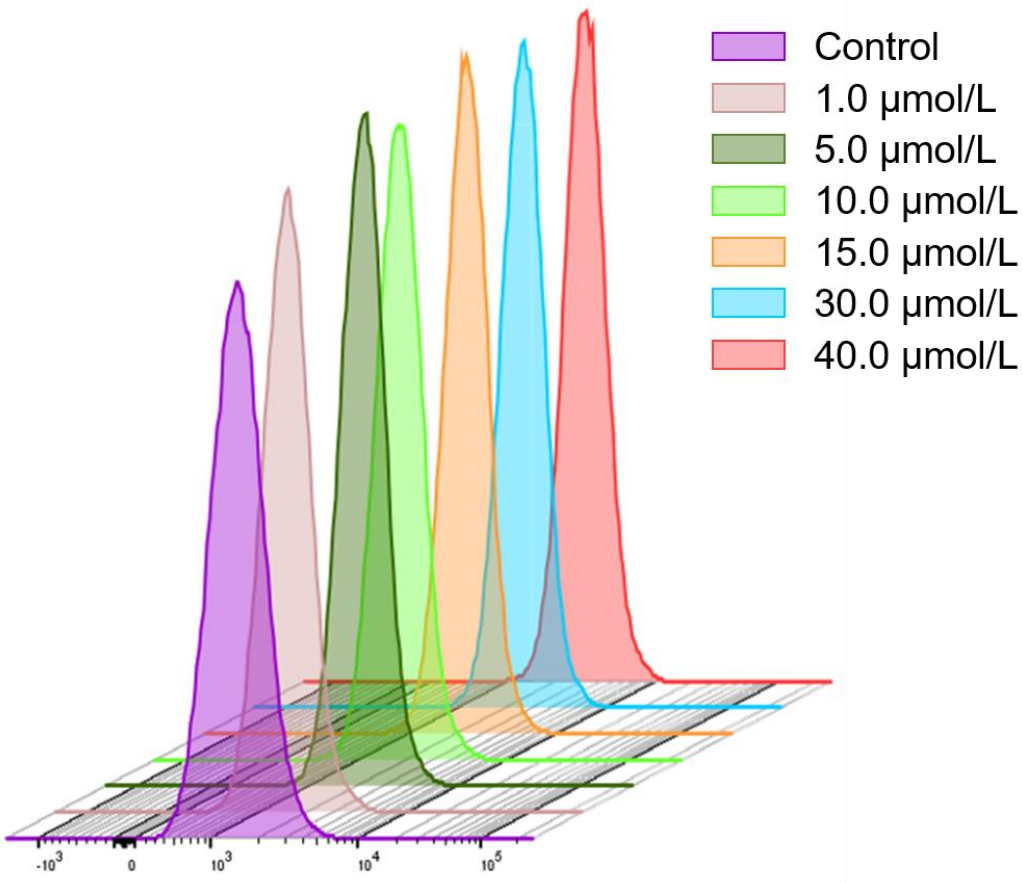

Supplementary Figure 25. Permeability of the **LDM** at concentrations of 1.0-40.0 μM in HepG2 cells. Three independent biological replicates were performed, and the results were similar. Source data are provided as a source data file.

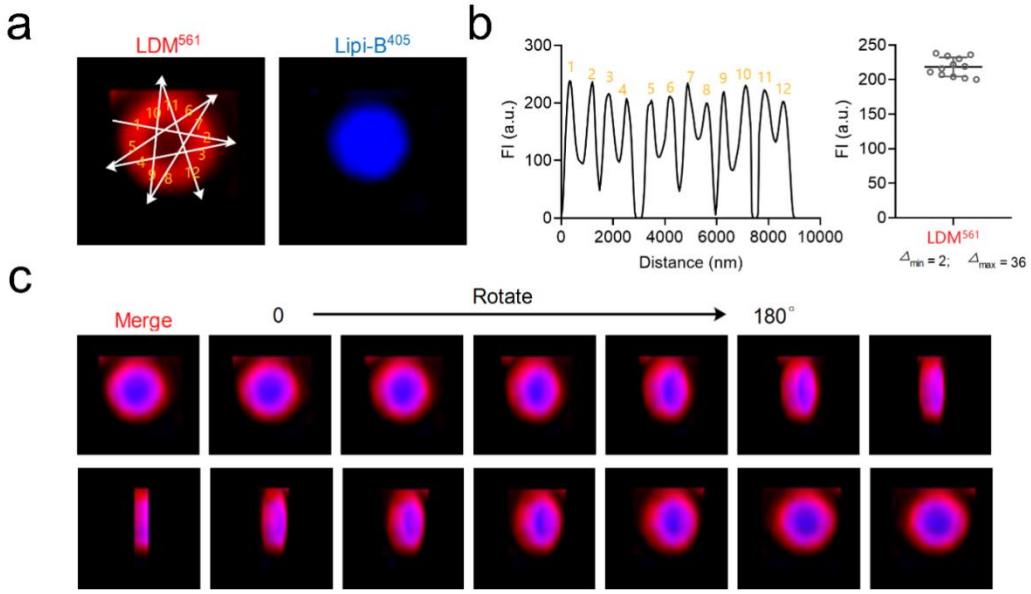

Supplementary Figure 26. Single LD SIM imaging was incubated with **LDM** and Lipi-B in HepG2 cells. (a) SIM images of HepG2 cells co-stained with commercial Lipi-B^{405} and **LDM**^{561} channel. (b) Compare the fluorescence intensity at 12 locations uniformly in the **LDM**^{561} channel of the membrane structure in (a). (c) Fluorescence imaging of single LDs with different rotation angles incubated with **LDM** and Lipi-B in HepG2 cells. Three independent imaging replicates were performed, and the results were similar. Source data are provided as a source data file.

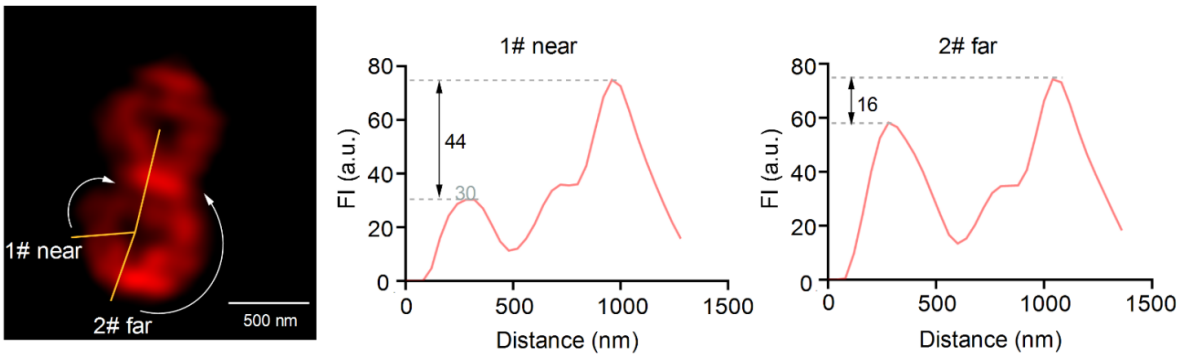

Supplementary Figure 27. SIM imaging of **LDM**^{561} channels of two LDs in contact with each other in HepG2 cells. SIM images of HepG2 cells co-stained with commercial **LDM**^{561} channel, the underlined areas are #1 near and #2 far. The curve analysis shows that the fluorescence intensity near the contact site is weaker than that far away from the contact site. Three independent imaging replicates were performed, and the results were similar. Source data are provided as a source data file.

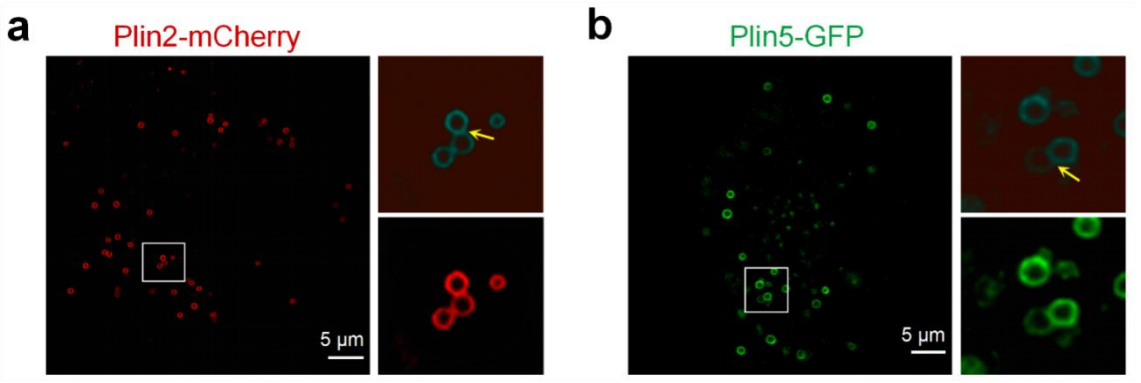

Supplementary Figure 28. Fluorescent labeling of LD membranes with uniformly distributed proteins. a. SIM images of LD membrane proteins Plin2 (mCherry-labeled) when LD membranes approached each other, with the yellow arrows indicating the approaching regions. Representative images. b. SIM images of LD membrane proteins Plin5 (GFP-labeled) when LD membranes approached each other, with the yellow arrows indicating the approaching regions. Representative images. Plin5-GFP channel: λex = 488 nm; Plin2 mCherry channel: λex = 561 nm, analyzed cells were obtained from three replicates. Three independent imaging replicates were performed, and the results were similar.

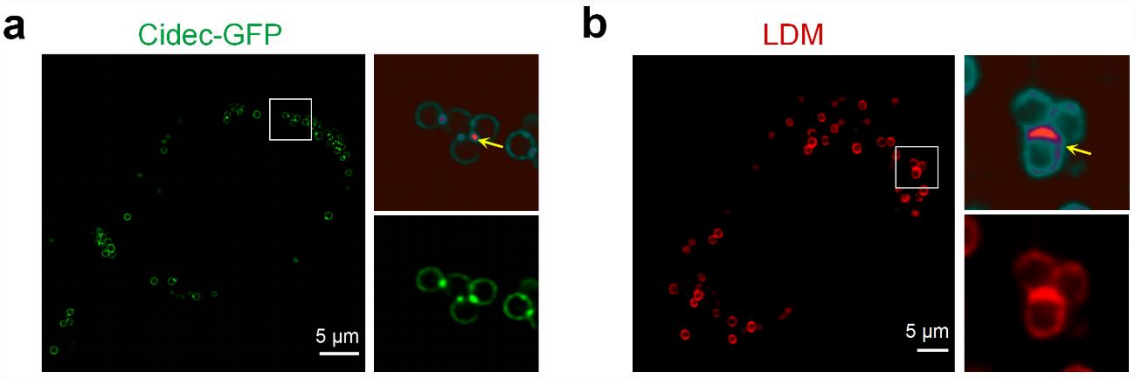

Supplementary Figure 29. Fluorescent labeling of LD Membranes by mobile distribution proteins and **LDM**. (a) SIM images of LD membrane proteins Cidec (GFP-labeled) when LD membranes approached each other, with the yellow arrows indicating the approaching regions. Representative images. (b) SIM images of **LDM** non-specifically labeled LD membrane proteins, when LD membranes approached each other, with the yellow arrows indicating the approaching regions. Representative images. Cidec-GFP channel: λ_{ex} = 488 nm; LDM channel: λ_{ex} = 561 nm. Three independent imaging replicates were performed, and the results were similar.

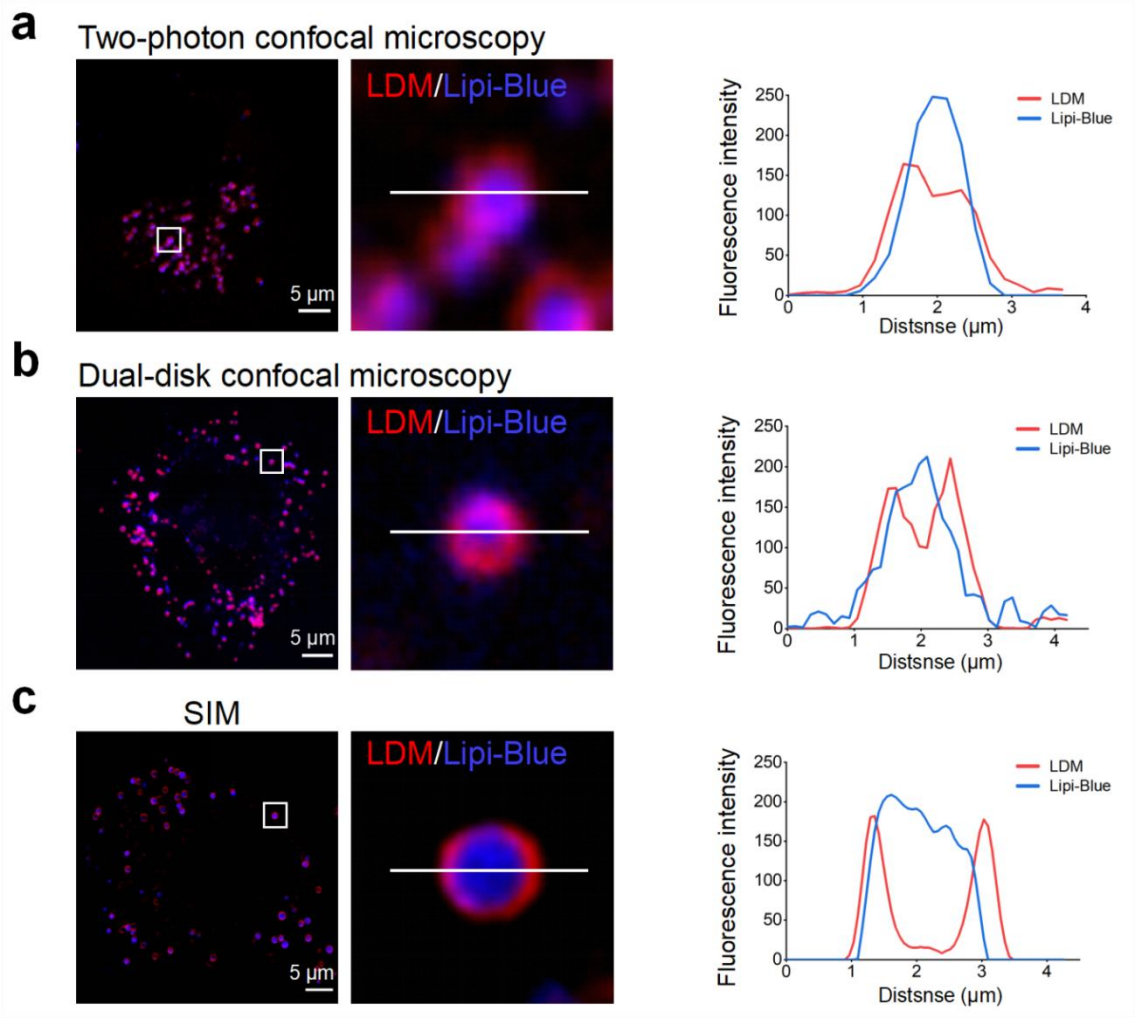

Supplementary Figure 30. Membrane of LDs labeled by **LDM** under different resolutions of microscopes. (a) Two-photon confocal microscopy images of LDs labeled with Lipi-Blue and the LD membrane protein layer labeled with **LDM**, as well as the fluorescence curve at the white line. Representative images. (b) Dual-disk confocal microscope images of LDs labeled with Lipi-Blue and LD membrane protein layer labeled with **LDM**, as well as the fluorescence curve at the white line. Representative images. (c) Super-resolution microscopy (SIM) images of LDs labeled with Lipi-Blue and LD membrane protein layer labeled with **LDM**, as well as the fluorescence curve at the white line. Representative images. Lipi-Blue channel: λ_{ex} = 405 nm; LDM channel: λ_{ex} = 561 nm. Three independent imaging replicates were performed, and the results were similar. Source data are provided as a source data file.

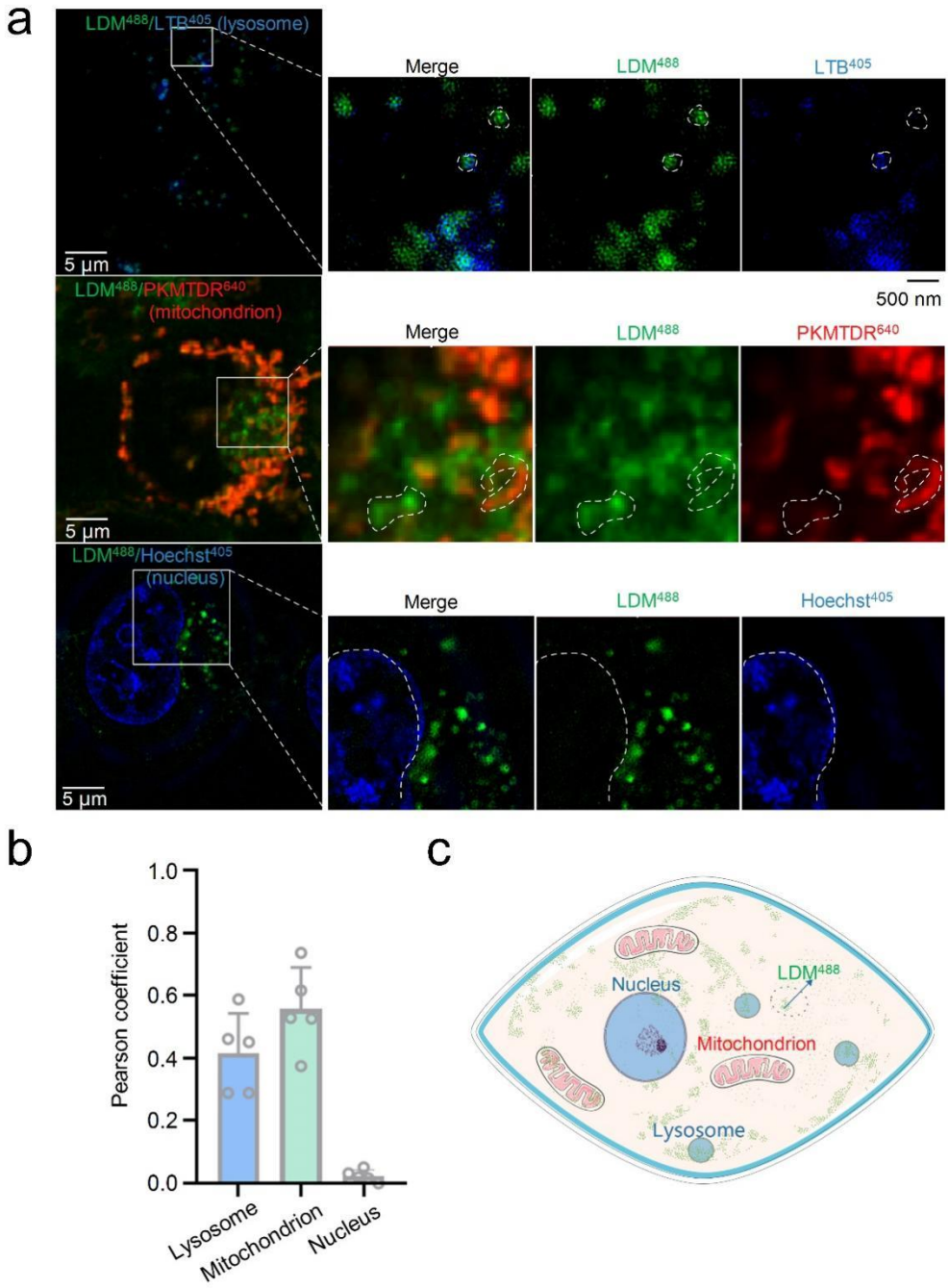

Supplementary Figure 31. Confocal imaging of **LDM**^{488} (10.0 μM) distribution within cells. HepG2 cells were incubated with lysosomes, mitochondria, and nuclear commercial dyes in a 37°C incubator for 30 min. Then the cells were associated with **LDM** (10.0 μM) incubate together for 40 min. (a) Colocalization imaging experiment of commercial Lysosome dye (LTB^{405}), commercial mitochondrial dye (PKMTDR) and Hoechst co-incubating cells with **LDM** respectively. (b) Data analysis of (a) (n = 5 cells). (c) Schematic diagram of the widespread distribution of **LDM** within cells. Created in BioRender. Shao, S. (2024) BioRender.com/m95t509. **LDM**^{488} channel: λ_{ex} = 488 nm; PKMTDR^{640} channel: λ_{ex} = 640 nm; LTB^{405}/Hoechst^{405} channel: λ_{ex} = 405 nm, scale bars 5 μm, the enlarged image, scale bars 500 nm. Three independent imaging replicates were performed, and the results were similar.

Source data are provided as a source data file.

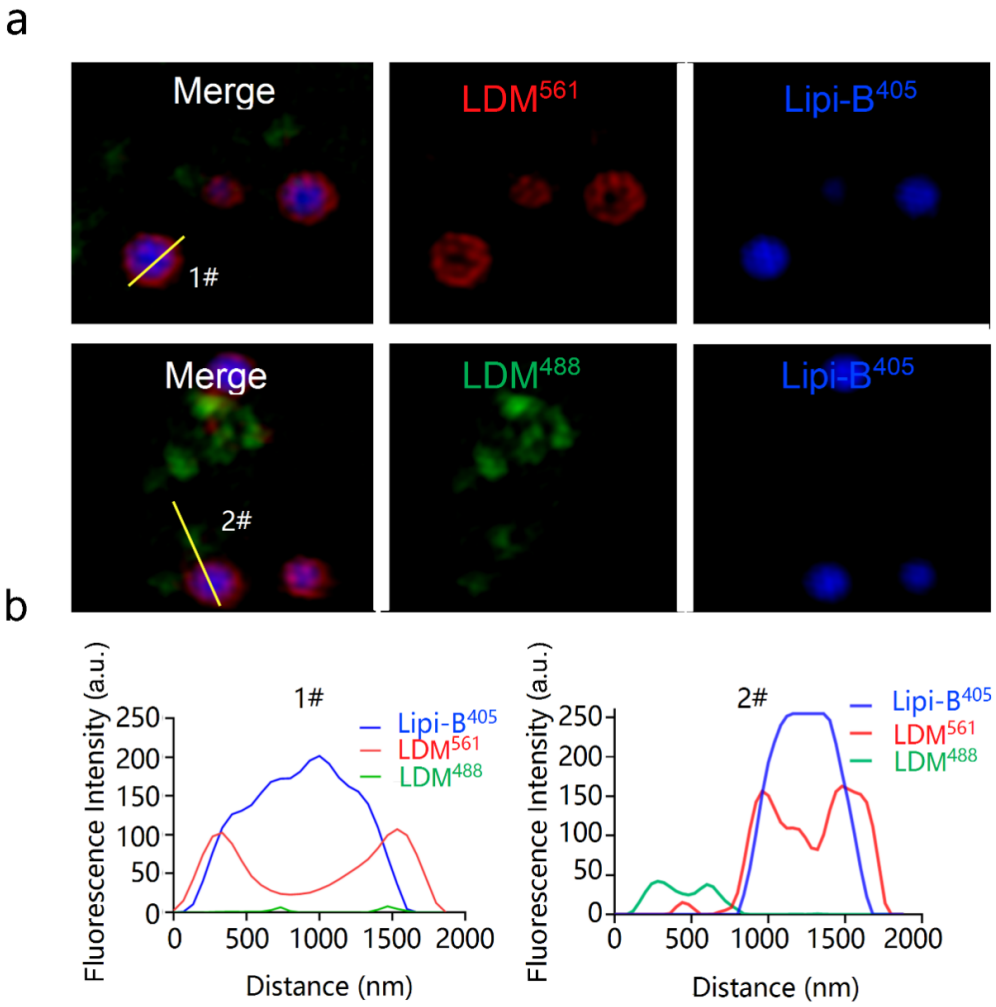

Supplementary Figure 32. SIM co-localization imaging experiment. HepG2 cells were incubated with blue commercial LD dye (Lipi-B^{405}) in a 37℃ incubator for 30 min. Then the cells were associated with **LDM** (10.0 μM) incubate together for 40 min. (a) SIM co-localization imaging experiment of blue commercial LD dye (Lipi-B^{405}) and **LDM** in HepG2 cells. **LDM**^{488} channel: λ_{ex} = 488 nm; **LDM**^{561} channel: λ_{ex} = 561 nm; Lipi-B^{405} channel: λ_{ex} = 405 nm, scale bars 500 nm. (b) Intensity data analysis of (a). Three independent imaging replicates were performed, and the results were similar. Source data are provided as a source data file.

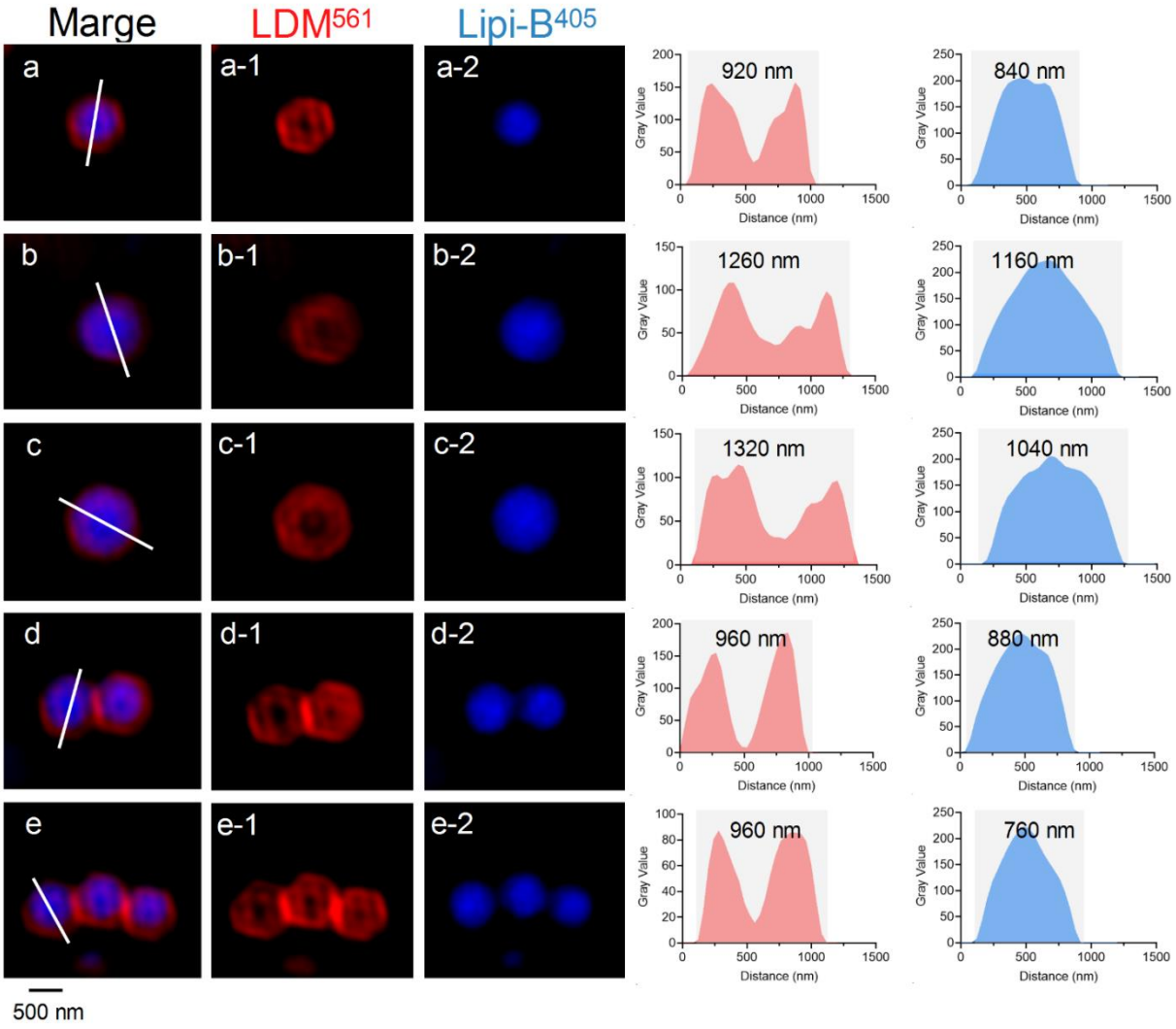

Supplementary Figure 33. The size of the LDs presented is significantly smaller than the **LDM**^{561}-labeled ring-like structure. HepG2 cells were incubated with blue commercial LD dye (Lipi-B^{405}) in a 37°C incubator for 30 min. Then the cells were associated with **LDM** (10.0 μM) incubate together for 40 min. **LDM**^{561} channel: λ_{ex} = 561 nm; Lipi-B^{405} channel: λ_{ex} = 405 nm, scale bars 500 nm. Left represent SIM imaging labeled with Lipi-B^{405} and **LDM**^{561} in HepG2 cells. Right: The corresponding line graph shows the analysis of fluorescence data in the underlined area, using ImageJ. Three independent imaging replicates were performed, and the results were similar.

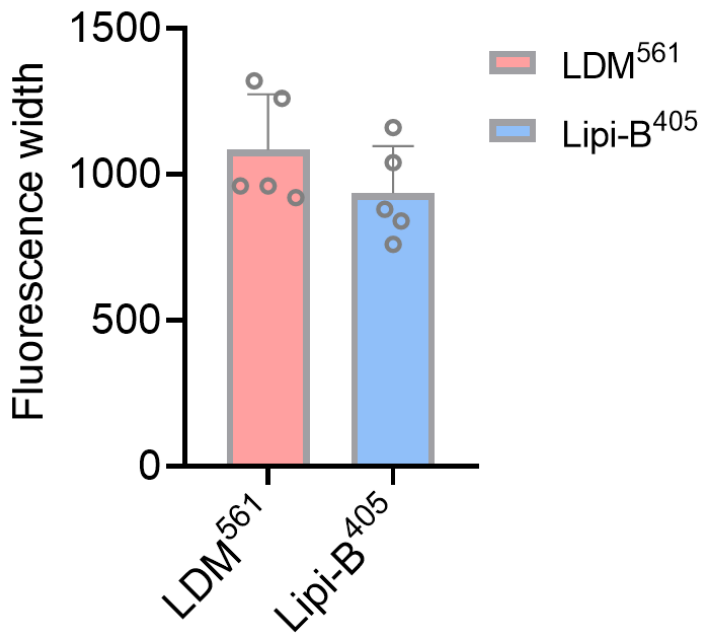

Supplementary Figure 34. Comparison of fluorescence regions between **LDM**^{561} channel membrane imaging and Lipi-B^{405} channel content dye SIM imaging, data from Supplementary Figure 23 (n = 5 cells). Three independent imaging replicates were performed, and the results were similar. Source data are provided as a source data file.

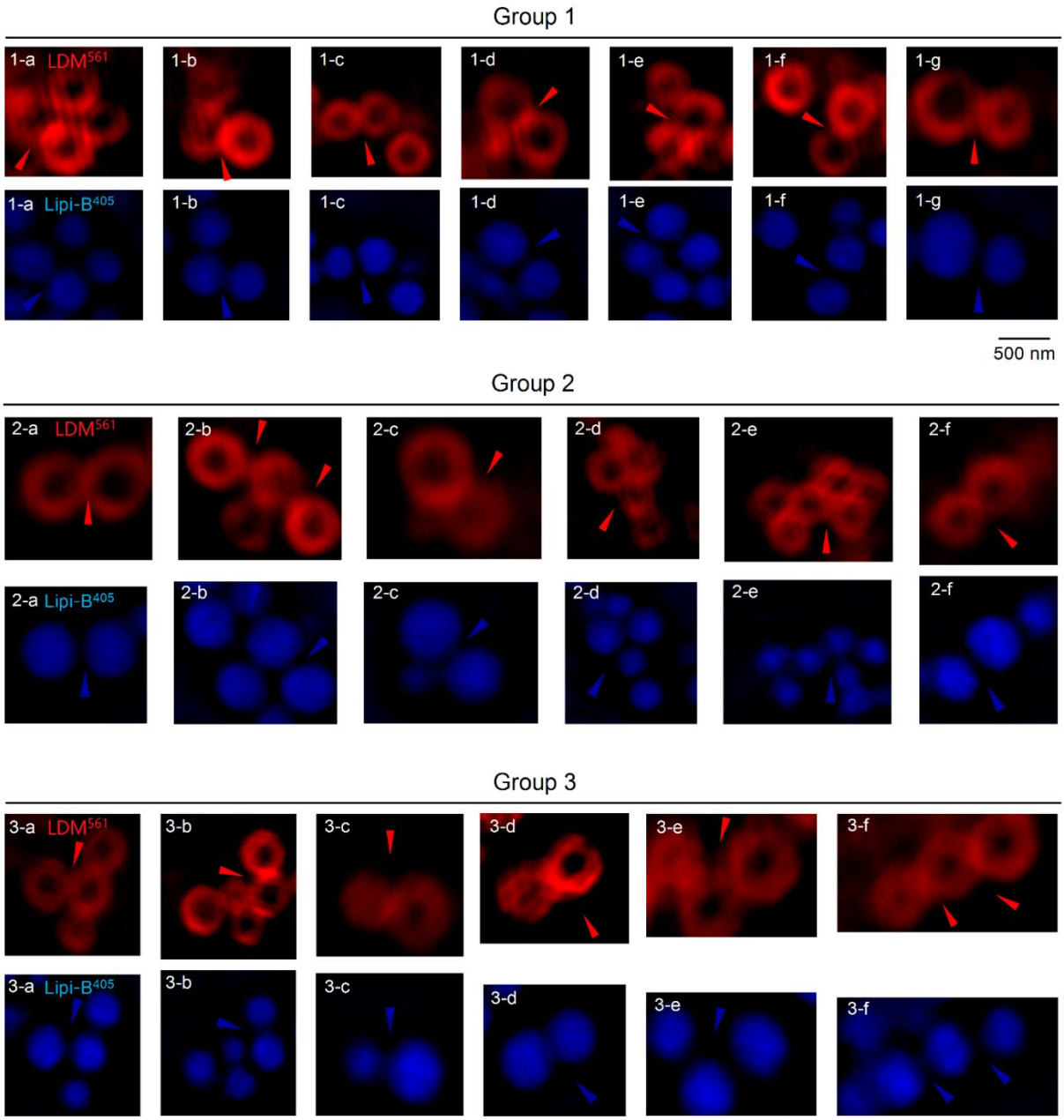

Supplementary Figure 35. The differences between membrane protein labeling strategies and content labeling strategies. The size of the Lipi-B^{405}-labeled blue spherical-like LD structure was significantly smaller than the **LDM**^{561}-labeled ring-like structure. When multiple LDs were in contact or fusion, they maintained independent spherical shapes. Lipi-B^{405} channel: λ_{ex} = 405 nm; **LDM**^{561} channel: λ_{ex} = 561 nm, scale bars 500 nm. Three independent imaging replicates were performed, and the results were similar.

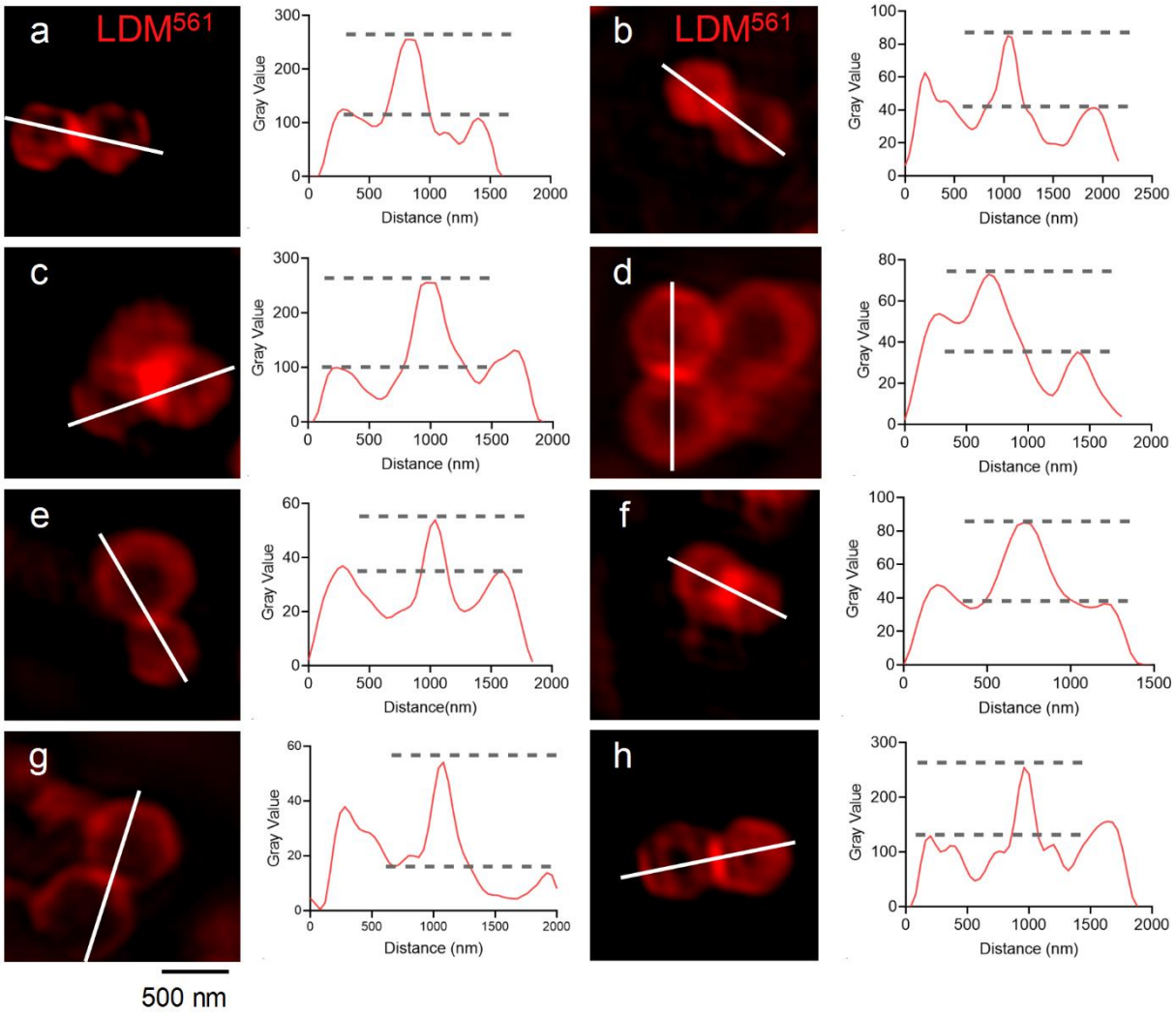

Supplementary Figure 36. **LDM**^{561}-labeled red fluorescent molecules show an uneven distribution at the contact site with multiple ring-like structures. (a-h) represent SIM imaging labeled with **LDM**^{561} in HepG2 cells. Compared to the noncontact area of the circular structure, the fluorescence intensity in the contact area of the circular structure significantly increases. The corresponding line graph shows the analysis of fluorescence data in the underlined area, using ImageJ. **LDM**^{561} channel: λ_{ex} = 561 nm, scale bars 500 nm. Three independent imaging replicates were performed, and the results were similar.

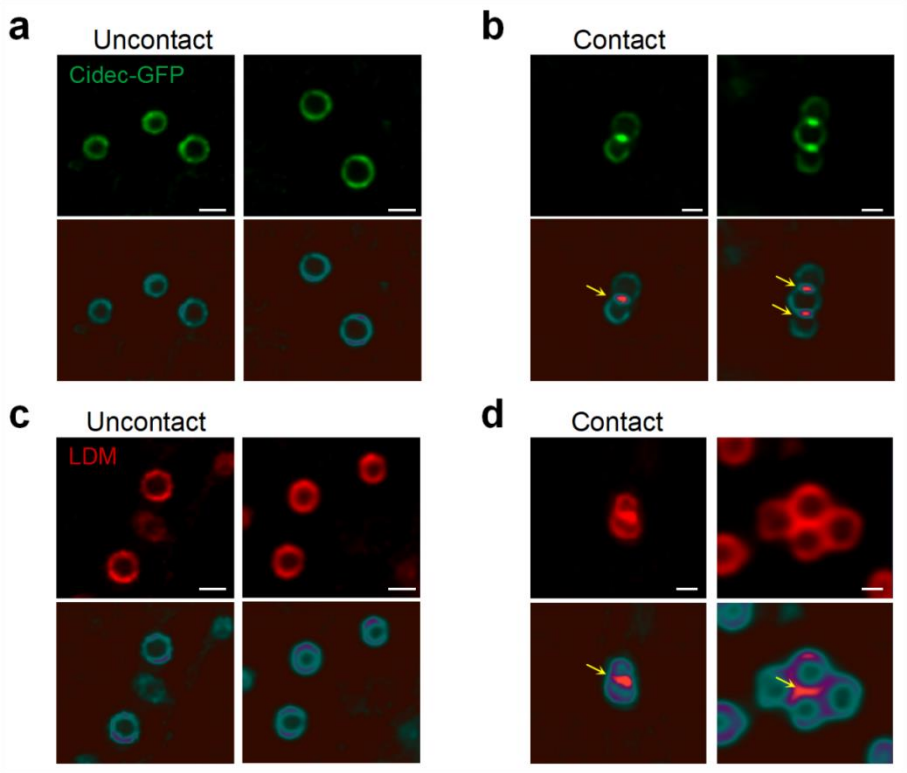

Supplementary Figure 37. The dynamics of Cidec-GFP and **LDM** labeled LD membrane proteins during non-contact and contact periods. (a) SIM image of the distribution of LD membrane protein Cidec-GFP on the surface of LDs (without membrane contact). Representative images. Scale bars, 1 μm. (b) Super-resolution microscopy image of the distribution of LD membrane protein Cidec-GFP on the surface of LDs (membrane contact), with the yellow arrows indicating the approaching regions. Representative images. Scale bars, 1 μm. (c) Super-resolution microscopy image of the distribution of LD membrane protein layer with **LDM** non-specific labeling on the LD (without membrane contact) membrane. Representative images. Scale bars, 1 μm. (d) Super-resolution microscopy image of the distribution of LD membrane protein layer with **LDM** non-specific labeling on the LD (membrane contact) membrane, with the yellow arrows indicating the approaching regions. Representative images. Scale bars, 1 μm. Cidec-GFP channel: λ_{ex} = 488 nm; LDM channel: λ_{ex} = 561 nm. Three independent imaging replicates were performed, and the results were similar.

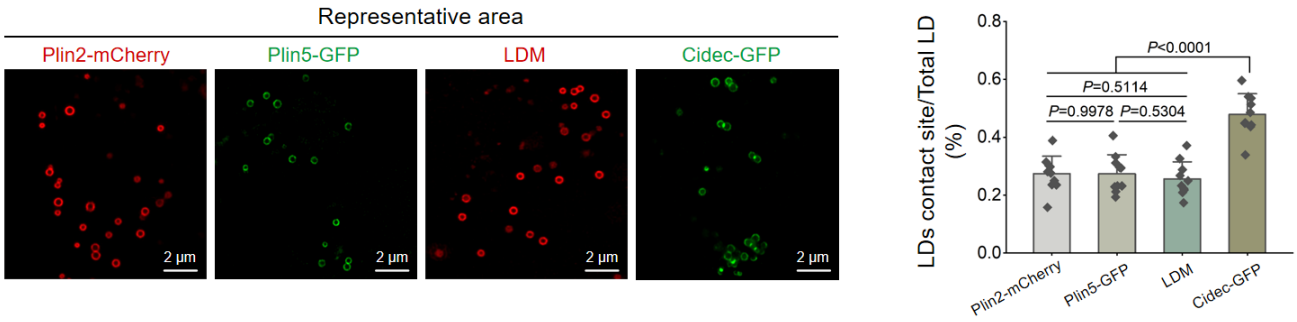

Supplementary Figure 38. SIM images of representative regions of LDs in HepG2 cells labeled with Plin2-mCherry, Plin5-GFP, **LDM**, and Cidec-GFP. (a) Representative images. (b) Quantitative analysis of LD-membrane contacts in HepG2 cells (n = 10 cells). Three independent imaging replicates were performed, and the results were similar. Statistical analysis was performed using two-tailed unpaired Student's t-test, and the data were presented as mean ± SD. $P < 0.05$ was considered statistically significant. Source data are provided as a source data file.

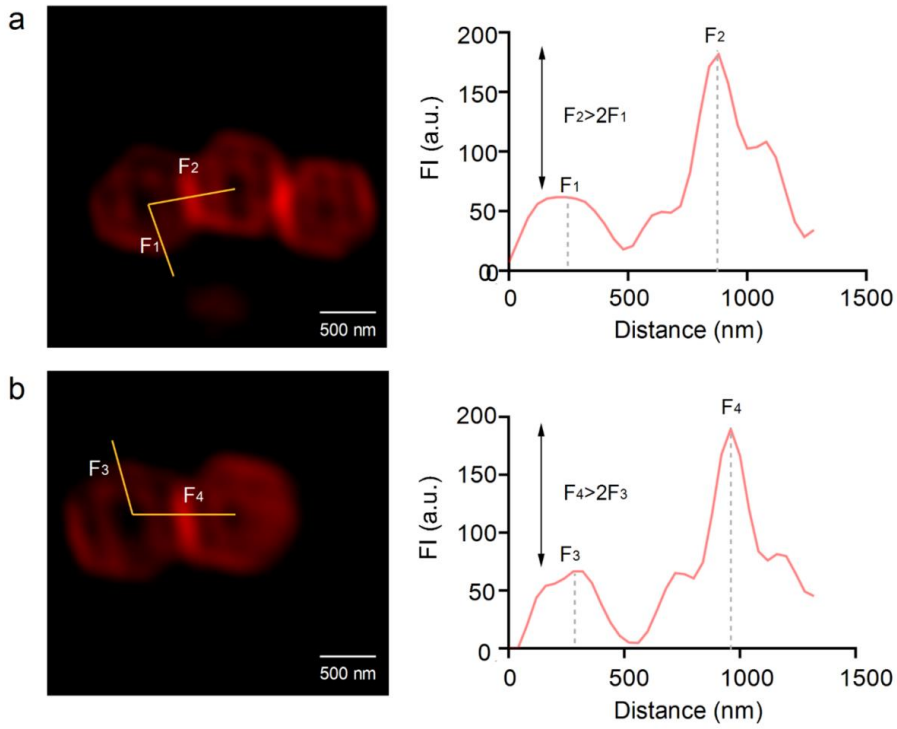

Supplementary Figure 39. SIM imaging of **LDM**^{561} channels of multiple LDs in contact with each other in HepG2 cells. (a-b) SIM images of HepG2 cells co-stained with commercial **LDM**^{561} channel. The fluorescence intensity at the marked area are represented by F_1, F_2, F_3 and F_4. The curve analysis shows that the fluorescence intensity of the contact site is more than twice that of the fluorescence intensity near the contact site (non-contact area). LDM channel: λ_{ex} = 561 nm. Three independent imaging replicates were performed, and the results were similar. Source data are provided as a source data file.

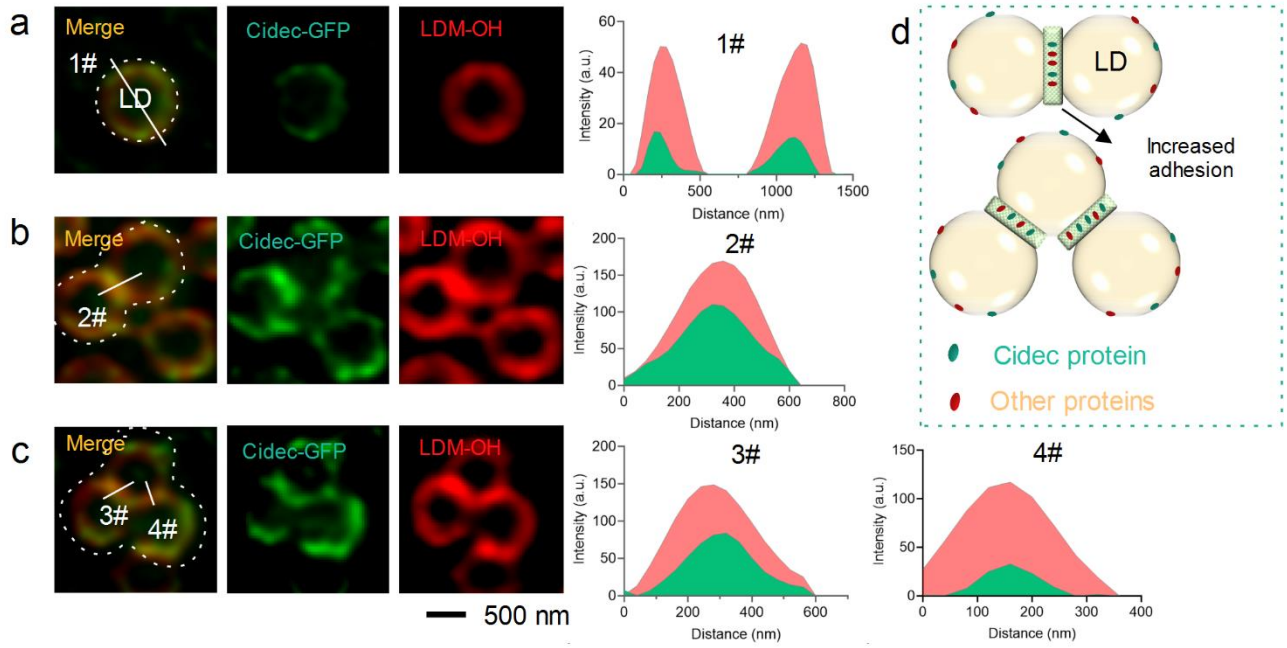

Supplementary Figure 40. A matching trend between the positioning of Cidec-GFP and the **LDM-OH**-labeled membrane protein in the LD membrane contact area. Analysis of the rotational motion of LDs and the involvement of multiple proteins in the generation of dynamic and permeable lipid fusion plates. (a-c) represent SIM imaging labeled with **LDM-OH** in Cidec-GFP plasmid transfected HepG2 cells. Co-localization of green fluorescent Cidec protein and red fluorescent **LDM**^{561}. Compared to the noncontact area of the circular structure, the fluorescence intensity in the contact area of the circular structure significantly increases. The corresponding line graph shows the analysis of fluorescence data in the underlined area, using ImageJ. **LDM**^{488} channel: λ_{ex} = 488 nm; **LDM**^{561} channel: λ_{ex} = 561 nm, scale bars 500 nm. (d) Schematic diagram of the presence of Cidec protein and other related proteins at the contact of LDs. Cidec-GFP channel: λ_{ex} = 488 nm. Three independent imaging replicates were performed, and the results were similar.

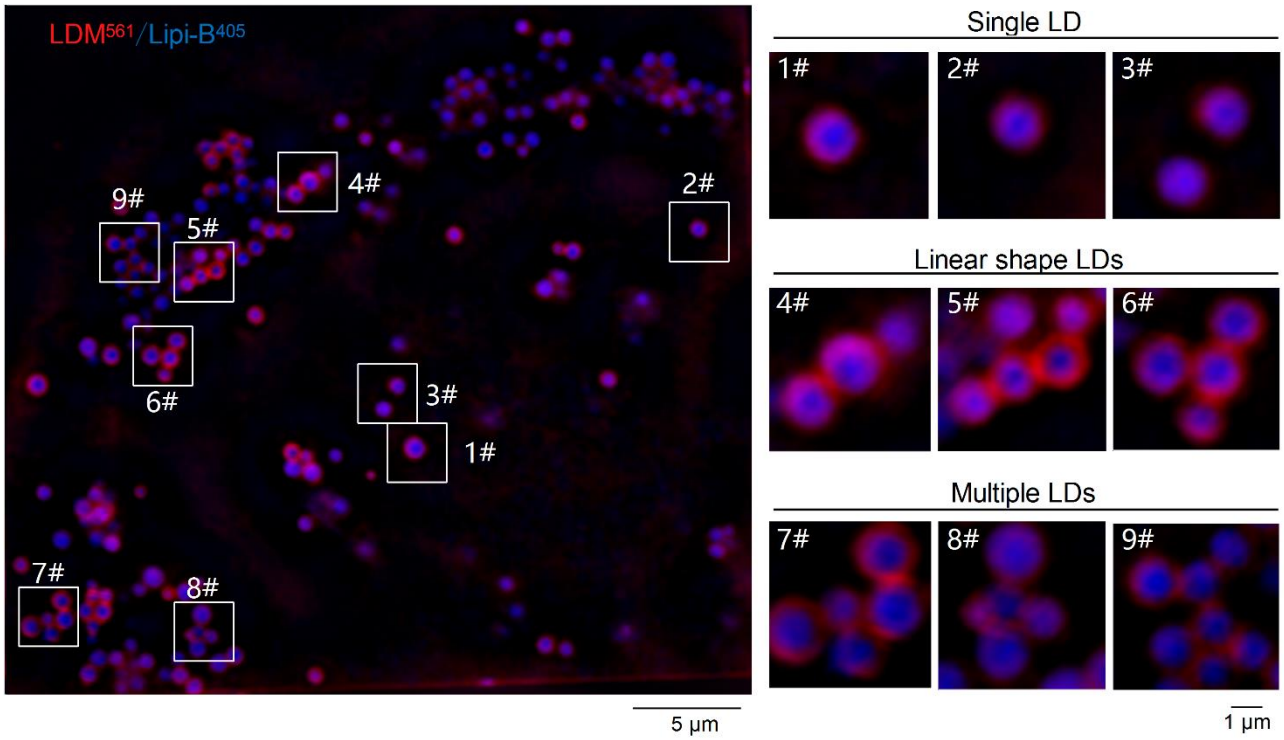

Supplementary Figure 41. SIM co localization imaging of HepG2 cells with sodium oleate (100.0 μM). HepG2 cells were pretreated with sodium oleate (100.0 μM) for 24 h. Then HepG2 cells were incubated with blue commercial LD dye (Lipi-B^{405}) in a 37℃ incubator for 30 min. Then the cells were associated with **LDM** (10.0 μM) incubate together for 40 min. **LDM**^{561} channel: λ_{ex} = 561 nm; Lipi-B^{405} channel: λ_{ex} = 405 nm, scale bars 5 μm, the enlarged image, scale bars 1 μm. Left represent SIM imaging labeled with Lipi-B^{405} and **LDM**^{561} in HepG2 cells. Right: SIM imaging show a significant increase in the number of membrane contacts, including single, multiple, and even linear membrane contacts. Three independent imaging replicates were performed, and the results were similar.

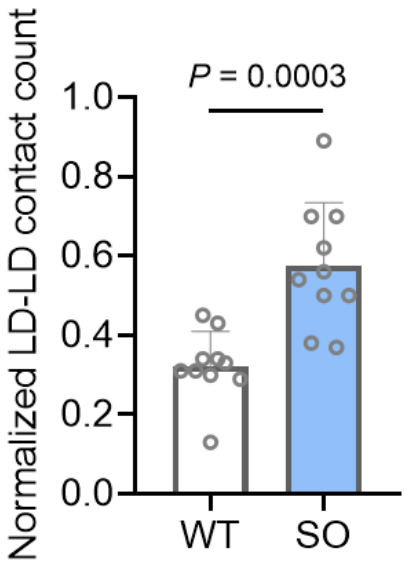

Supplementary Figure 42. Quantitative analysis of adhesion value changes of WT and sodium oleate in HepG2 cells (n = 10 cells). Three independent replicates were performed, and the results were similar. Statistical analysis was performed using two-tailed unpaired Student's t-test, and the data were presented as mean ± SD. $P < 0.05$ was considered statistically significant. Source data are provided as a source data file.

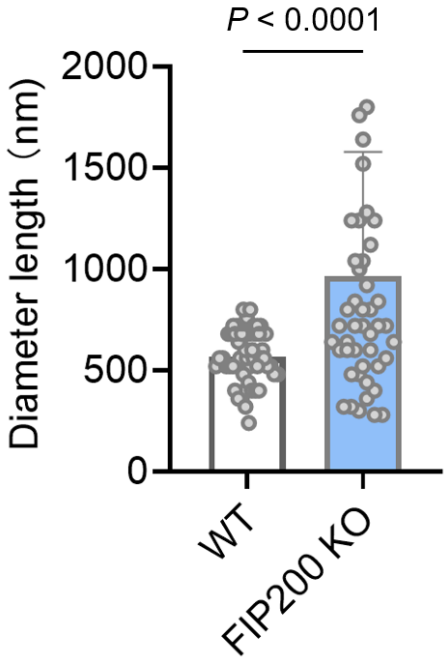

Supplementary Figure 43. Quantitative analysis of changes in adhesion values of WT and FIP200KO in HepG2 cells (n = 50 cells). Three independent replicates were performed, and the results were similar. Statistical analysis was performed using two-tailed unpaired Student's t-test, and the data were presented as mean ± SD. $P < 0.05$ was considered statistically significant. Source data are provided as

a source data file.

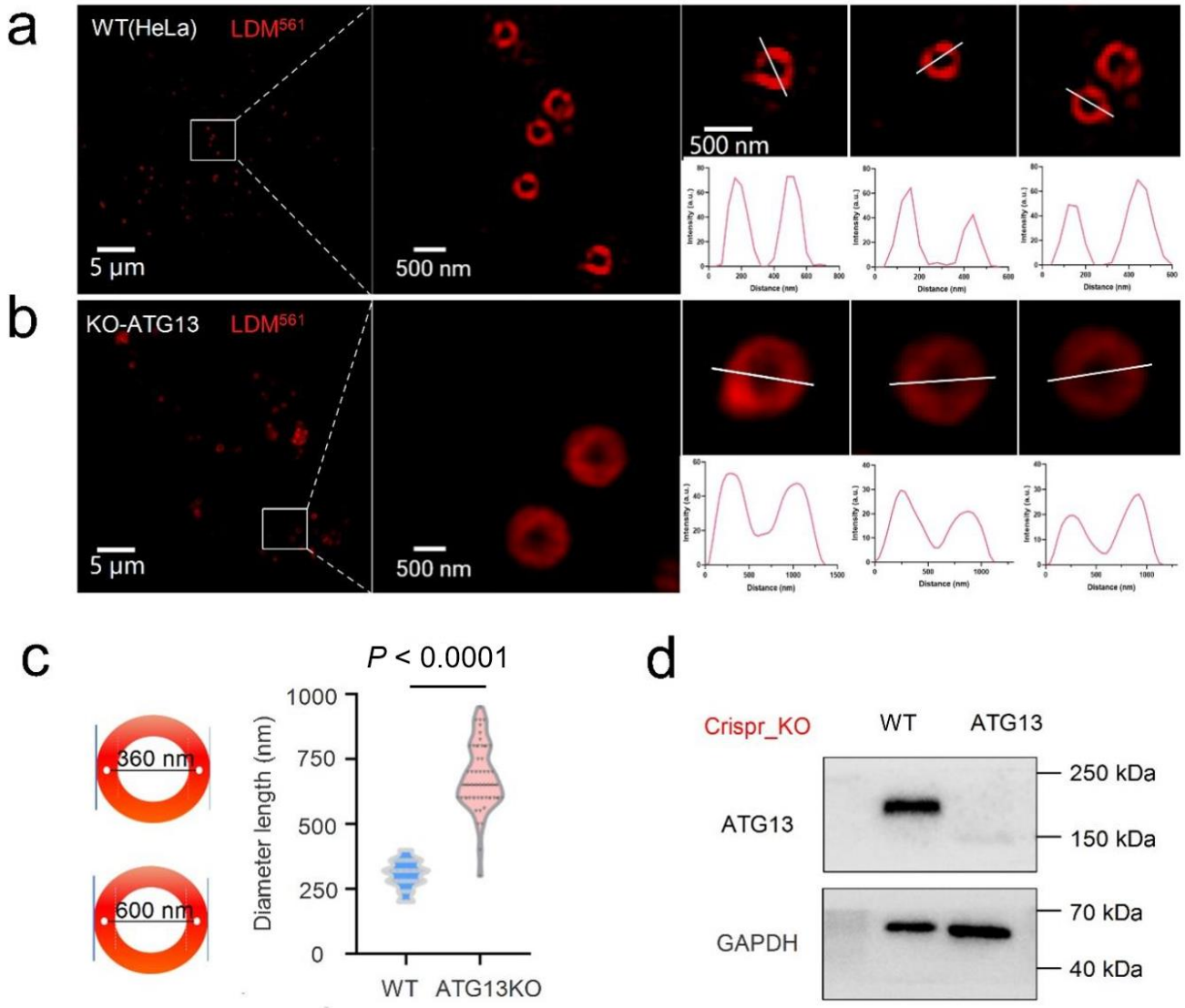

Supplementary Figure 44. LDs distribution in WT HeLa cells and ATG13KO HeLa cells. (a-b) LDs distribution in HeLa cells without treated or ATG13KO treatment, followed by incubation with **LDM** (10.0 μM, **LDM**^{561} channel: λ_{ex} = 561 nm, scale bars 5 μm, the enlarged image, scale bars 500 nm). (c) The diameter length of the LDs in (a and b) (n = 50 LDs). (d) Western blot for detecting ATG13 protein expression in HepG2 gene-edited cells. Three independent imaging replicates were performed, and the results were similar. Statistical analysis was performed using two-tailed unpaired Student's t-test, and the data were presented as mean ± SD. $P < 0.05$ was considered statistically significant. Source data are provided as a source data file.

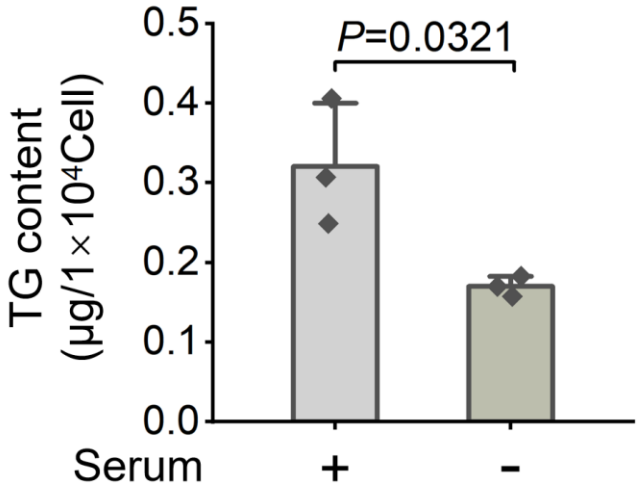

Supplementary Figure 45. Comparison of TG content in HepG2 cells under serum-fed and serum-free conditions (n = 3 cells). Three independent imaging replicates were performed, and the results were similar. Statistical analysis was performed using two-tailed unpaired Student's t-test, and the data were presented as mean ± SD. $P < 0.05$ was considered statistically significant. Source data are provided as a source data file.

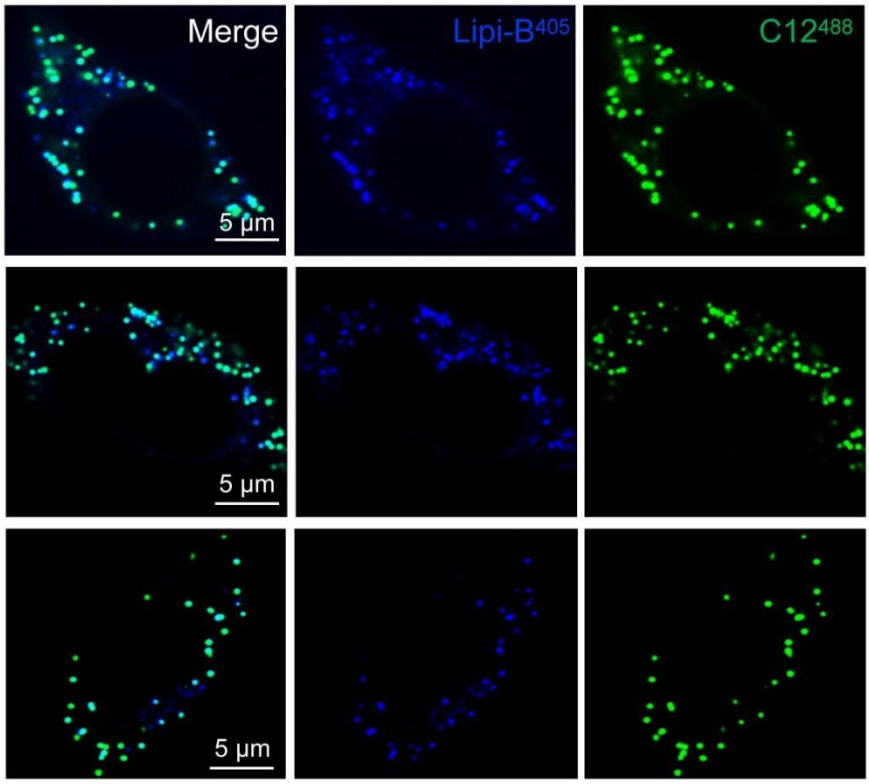

Supplementary Figure 46. Representative confocal images of co-localization of $C12^{488}$ and lipi-B^{405} on LDs in HepG2 cells. Lipi-B^{405} channel: λ_{ex} = 405 nm, Em max 447 nm (417-476 nm); $C12^{488}$ channel: λ_{ex} = 488 nm, Em max 510 nm (500-510 nm). Three independent imaging replicates were

performed, and the results were similar.

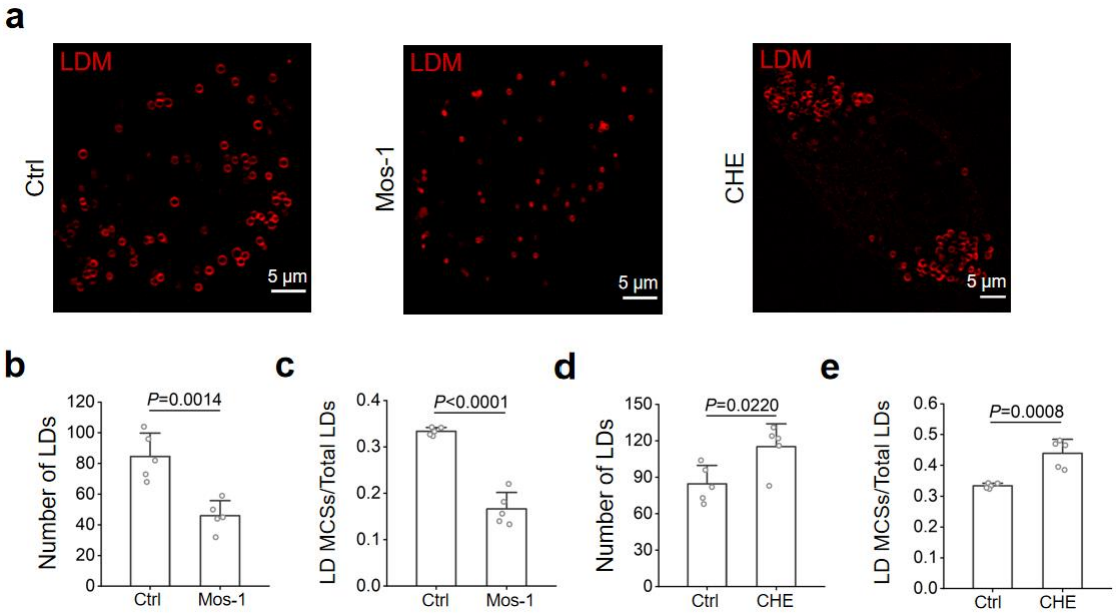

Supplementary Figure 47. Utilizing **LDM** to assess drug effects on LD and LD interaction. (a) The changes of LDs marked by **LDM** in the Ctrl group, the mussel oligosaccharides (Mos-1) group (100 μM, 24 h), and the chelerythrine (CHE) group (1 μM, 24 h). (b) Comparison of LD numbers between Ctrl and Mos-1 groups (n = 5 cells). (c) Comparison of the ratio of membrane contact sites (MCSs) to total number of LDs between Ctrl and Mos-1 groups (n = 5 cells). (d) Comparison of LD numbers between Ctrl and CHE groups (n = 5 cells). (e) Comparison of the ratio of MCSs to total number of LDs between Ctrl and CHE groups (n = 5 cells). LDM channel: λ_{ex} = 561 nm. Three independent imaging replicates were performed, and the results were similar. Statistical analysis was performed using two-tailed unpaired Student's t-test, and the data were presented as mean ± SD. $P < 0.05$ was considered statistically significant. Source data are provided as a source data file.

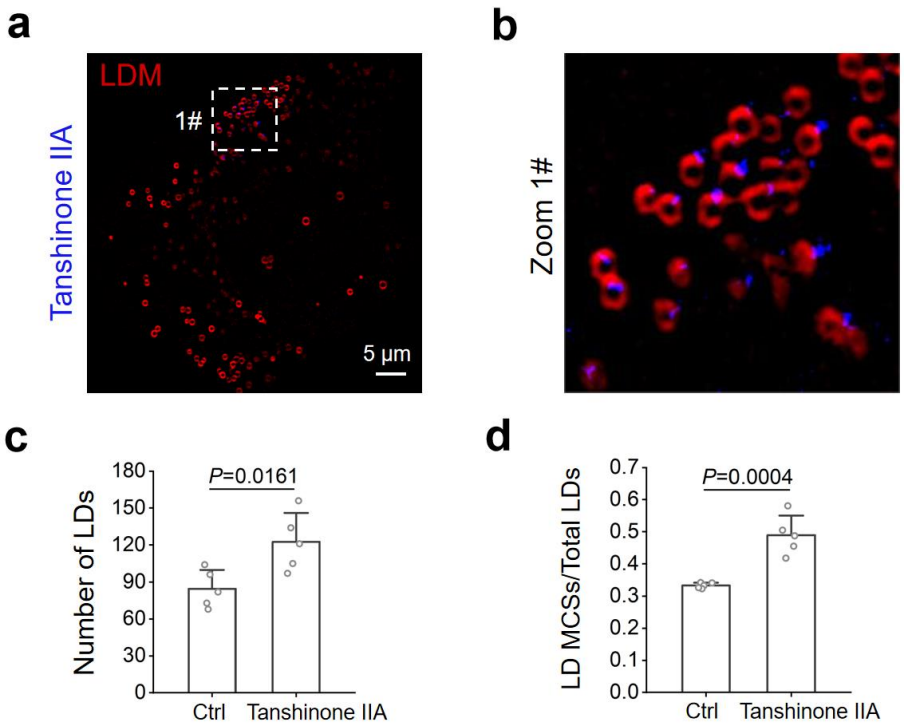

Supplementary Figure 48. Using **LDM** to evaluate the effect of drugs on LD interaction and check the drug's location in the LD membrane. (a-b) After treatment with 1 μM Tanshinone IIA (Blue) for 24 h, changes in LDs labeled by **LDM**. SIM imaging. Representative images. (c) Comparison of LD numbers between Ctrl and tanshinone IIA groups (n = 5 cells). (d) Comparison of the ratio of MCSs to total number of LDs between Ctrl and tanshinone IIA groups (n = 5 cells). Tanshinone IIA channel: λ_{ex} = 405 nm; LDM channel: λ_{ex} = 561 nm. Three independent imaging replicates were performed, and the results were similar. Statistical analysis was performed using two-tailed unpaired Student's t-test, and the data were presented as mean ± SD. $P < 0.05$ was considered statistically significant. Source data are provided as a source data file.

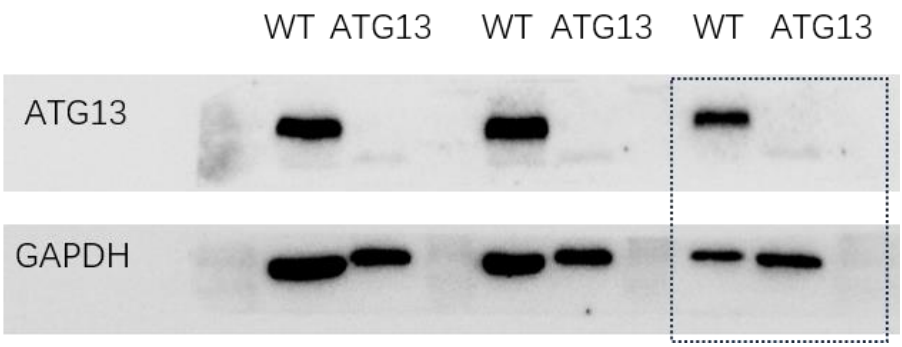

Supplementary Figure 43. (**d**) Western blot was used to detect ATG13 protein expression in HepG2 gene edited cells. The WT group consisted of normal HepG2 cells, while the FIP200 group showed no expression of ATG13 gene protein, indicating that the cells were FIP200 gene knockout cells. Three independent biological replicates were performed, and the results were similar.